

University of Mississippi

eGrove

Electronic Theses and Dissertations

Graduate School

1-1-2019

Use of seismic refraction in determining rock mass anisotropy

Mohammad Najmush Sakib Oyan

Follow this and additional works at: <https://egrove.olemiss.edu/etd>



Part of the [Geological Engineering Commons](#), and the [Geophysics and Seismology Commons](#)

Recommended Citation

Oyan, Mohammad Najmush Sakib, "Use of seismic refraction in determining rock mass anisotropy" (2019). *Electronic Theses and Dissertations*. 1776.

<https://egrove.olemiss.edu/etd/1776>

This Thesis is brought to you for free and open access by the Graduate School at eGrove. It has been accepted for inclusion in Electronic Theses and Dissertations by an authorized administrator of eGrove. For more information, please contact egrove@olemiss.edu.

USE OF SEISMIC REFRACTION IN DETERMINING ROCK MASS ANISOTROPY

A Thesis

Presented in partial fulfillment of requirements
for the degree of Master's in Engineering Science
in the Department of Geology and Geological Engineering
The University of Mississippi

by

MOHAMMAD NAJMUSH SAKIB OYAN

August 2019

Copyright Mohammad Najmush Sakib Oyan 2019

ALL RIGHTS RESERVED

ABSTRACT

Seismic refraction is a popular method used by geological/geotechnical engineers to understand subsurface conditions. This method, along with information collected from borings, produce a realistic image of the ground beneath us. The goal of this study is to define and test a set of procedures to use seismic refraction alone to create high quality images of subsurface conditions. The focus is on areas with several meters of soil overlain by bedrock. The application of these procedures will minimize construction costs by eliminating the need for multiple boreholes. The results show that two important criteria must be met for successful application of the method: a bedrock outcrop near the survey area and an area wide enough for geophone spacing to reach the bedrock. Seismic profiles are to be laid radially in an orthogonal position, preferably intersecting in the middle or in a quarter position but not at the end. Single channel geode is used for data acquisition and Rayfract® for data processing. Surfer® and Voxler® are used for graphical representations. Seismic refraction procedures are tested at two different sites: a road cut and an abandoned quarry. In one case (road cut) analysis did not show any anisotropy, which resulted from failure to meet the second criterion (geophone spacing). Analysis from second area (quarry) exhibited a clear anisotropic nature of bedrock, confirmed by observations on the exposed outcrop in the quarry. This is a qualitative study that can predict the orientation of major joint sets if the above criteria have been met.

DEDICATION

I dedicate this thesis to my parents; their inspirations from the other side of the world
always motivate me in countless ways.

ACKNOWLEDGEMENTS

I would like to convey my utmost gratitude to my advisor Dr. Adnan Aydin for teaching and guiding me throughout my whole master's carrier so much. I would like to express my special thanks to Dr. Lance D. Yarbrough for his valuable guidance about quarry locations and 3D graphical model software. I would also like to thank Dr. Louis G. Zachos for his valuable advice. I am very grateful to Dr. Gifford for providing materials and reviewing the part 'regional structural pattern' on Black Warrior basin carefully through her busy schedule.

We would like to express our gratitude to Mr. Jordan (Regional supervisor of Vulcan Materials Co.) for giving us permission to work in one of their quarries and assisting us through the whole work period. We are so grateful to Mr. Siegfried Rohdewald (Intelligent Resources Inc.) and Mr. Dieter Martin (GeoExpert) for their technical supports. I would like to thanks all the people who helped me in seismic data acquisition and processing: Dr. Adnan Aydin, Abdus Samad, Tanner Avery, Kausik Sarker, Steven Terracina and Bram Allen. I would like to thanks Sam Zachos for his continuous support on any software issues.

Last but not least, I would like to thank all other teachers, students, and staff members in The Department of Geology and Geological Engineering, who helped me to make this achievement possible.

TABLE OF CONTENTS

ABSTRACT.....	ii
DEDICATION.....	iii
ACKNOWLEDGEMENTS.....	iv
CHAPTER 1: INTRODUCTION.....	1
CHAPTER 2: BACKGROUND.....	3
ROCK MASS.....	3
SEISMIC REFRACTON METHOD.....	9
SEISMIC WAVE PROPAGATION THROUGH ROCK MASS.....	13
REGIONAL STRUCTURAL PATTERN.....	17
LITERATURE REVIEW.....	23
CHAPTER 3: METHODOLOGY.....	30
INITIAL TEST OF REFRACTION TOMOGRAOHY.....	30
LOCATION	30
GEOLOGY.....	30
STUDY PLAN	31

RESULTS AND DISCUSSIONS.....	32
CONCLUSIONS.....	33
CONCEPTUAL DESIGN OF STUDY.....	33
SITE SELECTION: STUDY AREA 1.....	35
SITE SELECTION: STUDY AREA 2.....	35
DATA COLLECTION.....	37
SEISMIC REFRACTION DATA ANALYSIS SOFTWARE: RAYFRACT®.....	38
NOISE ANALYSIS.....	39
CHAPTER 4: RESULTS.....	42
VELOCITY TOMOGRAM FROM FIRST STUDY AREA.....	42
VELOCITY TOMOGRAM FROM SECOND STUDY AREA.....	43
3D FENCE DIAGRAM (VELOCITY).....	48
3D FENCE DIAGRAM (ROCK MASS QUALITY, Q).....	49
CHAPTER 5: DISCUSSIONS AND CONCLUSIONS.....	51
DISCUSSIONS.....	51
CONCLUSIONS.....	56

REFERENCES.....	58
LIST OF APPENDICES.....	67
APPENDIX A.....	68
APPENDIX B.....	69
APPENDIX C.....	71
VITA.....	83

LIST OF TABLES

Table 1: Rock mass discontinuity types.....	3
Table 2: V_S/V_P for different rock types.....	11
Table 3: Effect of foliation, cleavage, and schistosity on V_P . Both dry and saturated state	24
Table 4: Rock mass quality, Q parameters.....	55
Table C1: Survey information.....	73

LIST OF FIGURES

Figure 1: Structural discontinuity (faults).....	4
Figure 2: Metamorphic discontinuity (cleavage).....	4
Figure 3: Sedimentary discontinuity (bedding planes).....	5
Figure 4: Igneous discontinuity (sills and dykes).....	5
Figure 5: Rock mass description.....	7
Figure 6: Integration of rock quality Q-VP-E _{mass} in a model that incorporates depth, porosity and rock strength adjustments.....	8
Figure 7: Basic components of a seismic refraction survey.....	9
Figure 8: Body waves propagation and particle vibration (top: P-wave, bottom: S-wave).....	10
Figure 9: Surface waves propagation and particle vibration (top: Rayleigh-wave, bottom: Love- wave).....	12
Figure 10: Partitioning of wave energy among reflected and refracted P and S-waves.....	14
Figure 11: Partitioning incident of P wave.....	15
Figure 12: Outline of regional structural setting of Black Warrior basin.....	17
Figure 13: The geologic map of Mississippi.....	19

Figure 14: Structural features of Mississippi.....	20
Figure 15: North-south cross section A-A' from the Mississippi-Tennessee state line to Horn Island in the Gulf of Mexico.....	21
Figure 16: Velocity anisotropy of slate due to cleavage.....	23
Figure 17: Velocity anisotropy with gypsum samples with deformable cracks and two jointed granite sites in Japan.....	25
Figure 18: sensitivity of the velocity anisotropy towards uniaxial loading.....	26
Figure 19: Seismic observation scheme showing geophone spread and source point arrangement e.g. solid line L7= Line 7 occupied by 12 geophones at 2m spacing and recorded from shot positions S0, S6, S7 and S8. 'Fan' arrangement (dashed line) of geophones at S1 to S9 were recorded from the source positions.....	27
Figure 20: Azimuthal V_P anisotropy at jointed limestone sites in Lincolnshire, England.....	28
Figure 21: Change in velocity anisotropy for different frequencies of jointing.....	29
Figure 22: Location of the segment of levee at Tunica, Mississippi.....	30
Figure 23: Sample diagram from initial study.....	32
Figure 24: Schematic diagram hypothetical survey plan.....	34

Figure 25: First study area. 1) Aerial view of the area, 2) Survey plan, 3 & 4) Field observation red elliptical boundary. The red arrows are indicating two features along the cut-face.....	36
Figure 26: Second study area. 1) Aerial view of the area, 2) Survey plan and 3 & 4) Field observation.....	37
Figure 27: SEG-2 to ASCII Decoder.....	40
Figure 28: The apparent straight line in the seismic trace was not straight at all.....	40
Figure 29: Study area 1 (Road cut site): Line 1 tomogram.....	42
Figure 30: Study area 1 (Road cut site): Line 2 tomogram.....	43
Figure 31: Study area 2 (Dolomite quarry), Intersection 1: Line 1 tomogram.....	44
Figure 32: Study area 2 (Dolomite quarry), Intersection 1: Line 2 tomogram.....	45
Figure 33: Study area 2 (Dolomite quarry), Intersection 2: Line 3 tomogram.....	46
Figure 34: Study area 2 (Dolomite quarry), Intersection 2: Line 4 tomogram.....	47
Figure 35: Study area 1 (Road cut site), Velocity fence diagram.....	48
Figure 36: Study area 2 (Dolomite quarry), Intersection 1: Velocity fence diagram.....	48
Figure 37: Study area 2 (Dolomite quarry), Intersection 2: Velocity fence diagram.....	49
Figure 38: Study area 1 (Road cut site): Fence diagram of Q value (Rock mass quality, Q).....	49

Figure 39: Study area 2 (Dolomite quarry), Intersection 1: Fence diagram of Q value (Rock mass quality, Q).....	50
Figure 40: Study area 2 (Dolomite quarry), Intersection 2: Fence diagram of Q value (Rock mass quality, Q).....	50
Figure 41: Observed joint system.....	54
Figure 42: Predicted joint system (Both white solid and dashed lines).....	54
Figure A1: The 1993 updated Q-support chart for selecting permanent B+S(fr) reinforcement and support for tunnels and caverns in rock.....	68
Figure B1: Riverside tomogram.....	69
Figure B2: Landside tomogram.....	70
Figure C1: Edit profile display.....	71
Figure C2: Import shot display (Left) and Shot information display (Right).....	72
Figure C3: Shot gather display.....	73
Figure C4: Shot breaks display.....	76
Figure C5: WET parameter display.....	77
Figure C6: File import display (Left) and Network manager (Right).....	80
Figure C7: Property manager (for scatter plot: left and for data: right).....	80

CHAPTER 1

INTRODUCTION

Anisotropy is a broad term which can be applied to subjects such as rock strength, permeability, and seismic velocity. In this study, the emphasis is put on seismic velocity anisotropy exclusively due to discontinuities such as joints and fractures. No anisotropy due to lithological changes will be considered in this study. One of the key features of the rock strength is its anisotropic behavior. The primary objective of this study is to evaluate the effectiveness of a quick, budget-friendly, non-destructive seismic refraction method for determination of subsurface anisotropic conditions.

In the seismic refraction method, direct and back propagating waves produced by a source are received and analyzed to build a model of the ground. This method is based on the gradual increase of seismic wave velocity with depth. A low-velocity layer between two high-velocity zones cannot be seen or a thin, high-velocity layer can completely mask the layers below it, even with wider geophone spacing. Existence of slow velocity channel or high-velocity zone can push or pull the target horizon, which in our case is bedrock, respectively (Armstrong, McAteer, & Connolly, 2001). Only major joint sets are considered in this study because seismic waves have a large wavelength which is comparable in size with large discontinuities like joints. We have used P-waves in our study, which are sensitive to the discontinuities of the rock mass as well as its saturation. Earlier work has been done on The Confederate Cemetery located within The

University of Mississippi premises and also on a segment of the Coldwater River located at Tunica, Mississippi (Bohara et al., 2017; Rhodes et al., 2017 and 2018). In the cemetery, buried bodies University of Mississippi premises and also on a segment of the Coldwater River located at Tunica, Mississippi (Bohara et al., 2017; Rhodes et al., 2017 and 2018). In the cemetery, buried bodies were looked for and, in the levee, the cover quality on the core was examined. Grid patterns have been adopted there.

When identifying anisotropic features within rock mass a different pattern i.e. radial proves useful in this kind of study (Nunn, Barker, & Bamford, 1983; Leary & Henyey, 1985). The velocity tomogram changes as its orientation relative to major joint sets changes. Profiles that run along the joint sets predict bedrock shallower than the profiles that run normal to joint sets. Profiles that are not laid down at any angle other than orthogonal position show some intermediate images of subsurface within this boundary. Due to the non-unique characteristic of the seismic refraction method, an exposed cut-slope or outcrop is necessary to make our findings valid because non-uniqueness is the fundamental characteristic of the seismic inversion algorithm (palmer, 2010).

CHAPTER 2

BACKGROUND

Rock mass

The rock mass is defined as an interlocked aggregate of rock blocks separated or bounded by planar discontinuities. Discontinuities are characterized in four types:

Table 1: Rock mass discontinuity types

Rock Mass Discontinuities	
Sedimentary discontinuity	Bedding planes
	Sedimentary structures (mud cracks, ripple marks, cross beds etc.)
Structural discontinuity	Faults
	Joints
	Fissures and cracks
Metamorphic discontinuity	Foliation
	Cleavage
Igneous discontinuity	Cooling joints
	Flow contacts
	Intrusive contacts
	Dikes
	Sills
	Veins

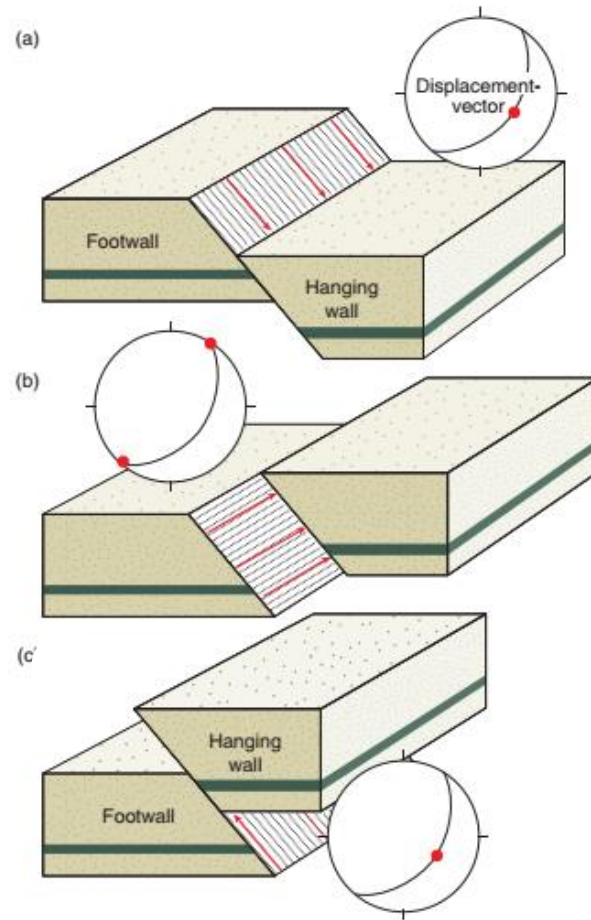


Figure 1: Structural discontinuity (faults) (Fossen, 2010).



Figure 2: Metamorphic discontinuity (cleavage) (Fossen, 2010).



Figure 3: Sedimentary discontinuity (bedding planes) (Boggs, 2006).

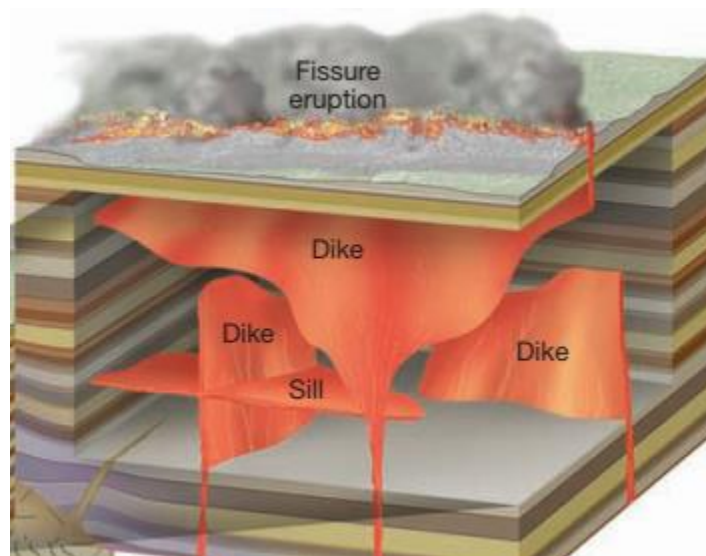


Figure 4: Igneous discontinuity (sills and dykes) (Lutgens & Tarbuck, 2012).

Normally rock masses located with first several hundreds of meters act as a discontinuous medium due to the presence of these features. A description of rock mass based on these discontinuities is necessary to determine the rock mass strength and for the safety of construction. This description mainly helps to understand its mechanical behavior and to establish an empirical

formula. Such a well-developed empirical formula is rock mass quality, Q , which is described by six parameters of discontinuity (Barton, Lien, & Lunde, 1974).

$$Q = \frac{RQD}{J_n} \times \frac{J_r}{J_a} \times \frac{J_w}{SRF} \quad 1$$

Where, RQD = rock quality designation, the percentage of cored length that yields core in segments longer than 10 cm (4 in) assuming the core diameter is 50 mm (2 in). More general yielded core segments length should be longer than twice of its diameter; J_n = Joint set number, J_r = Joint roughness number, J_a = Joint alteration (filling) number, J_w = Joint water reduction factor, SRF = Stress reduction factor, a rating for faulting, strength/stress ratio in the hard massive rock mass and for squeezing/swelling.

The first term of this relation RQD/J_n represents the overall structure of rock mass and it's a crude measure of the relative block size. The second term J_r/J_a represents the relative friction angle of the least favorable joint sets which is an approximation of actual shear strength of the joints with different combinations of wall roughness and filling materials. It is found that the inverse tangent of this term gives the actual peak sliding angle of friction. The last term J_w/SRF is a complicated empirical factor describing the active effective stress. The above relation was developed using 212 Scandinavian tunneling case histories and subsequently applied in various application. Combining the data of cross-hole seismic tomography 60m span Olympic ice-hockey cavern at Gjøvik, Norway with Q system application and in situ testing results at the Yellow River

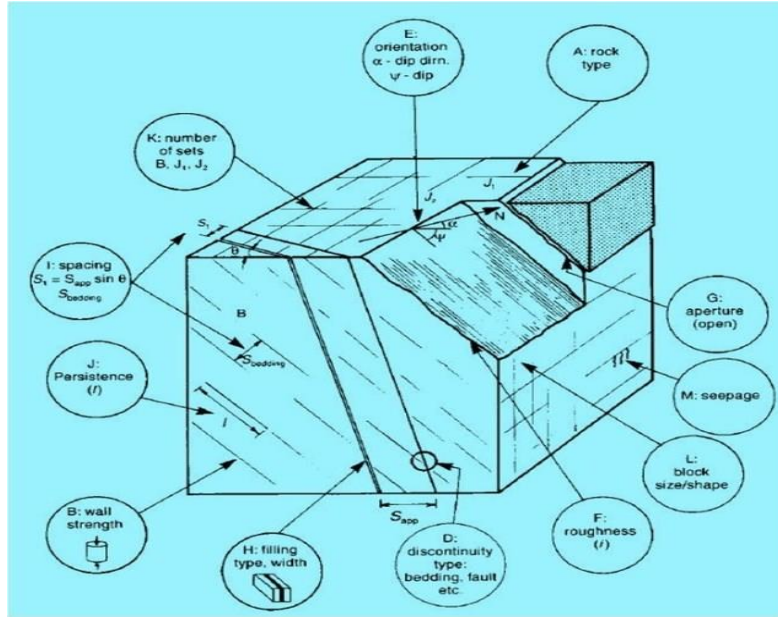


Figure 5: Rock mass description (Wyllie, 1999).

Xiaolangdi dam site, NGI (Norwegian Geological Institute) proposed a correlation between Q and P-wave velocity for ‘hard’ rock (Barton, 1991).

$$V_P = 3.5(Km. s^{-1}) + \log_{10} Q \quad 2$$

Where, V_P is in km/s. Each 1 km/s increase in seismic P-wave velocity will increase Q -value by 10. Above equation was generalized to include weaker and stronger than the assume ‘hard’ rock ($\sigma_c = 100$ MPa). A new correlation was established between nominal rock strength ($\sigma = 100$ MPa) to the ‘hard’ rock (Barton, 2002). The rock mass quality Q value for ‘hard’ rock was denoted by Q_c in this relation.

$$Q_c = Q \times \frac{\sigma_c}{100} \quad 3$$

Where σ_c is the uniaxial compressive strength of rock and it is describing the quality of rock mass. This parameter strongly correlates with Young’s modulus and has a tendency to correlate with the density and porosity (Lashkaripour & Passaris, 1995; Barton, 2002). V_P has a

proportional relation to the density and Young's modulus and inverse relation to porosity (Iliev, 1966; Grujić, 1974.). So, a positive correction for depth and negative correction for porosity is necessary to cover both high and low velocity, and significant and negligibly porous zone. V_P usually increases with depth even having unchanged RQD, joint frequency and Q-value of the rock mass. This is due to the 'seismic closure' that takes place in weak rocks at shallow depth and in stronger rocks at great depth.

$$V_P = 3.5 \left(\frac{km}{s} \right) + \log_{10} Q_c \quad 4$$

Above equation is a revised version of equation 2 which has maintained consistency with the soft rock when both depth and porosity correction was applied. The following graph is an integration of seismic P-wave velocity, Q_c and deformation modulus with depth, porosity correction (Barton, 2002).

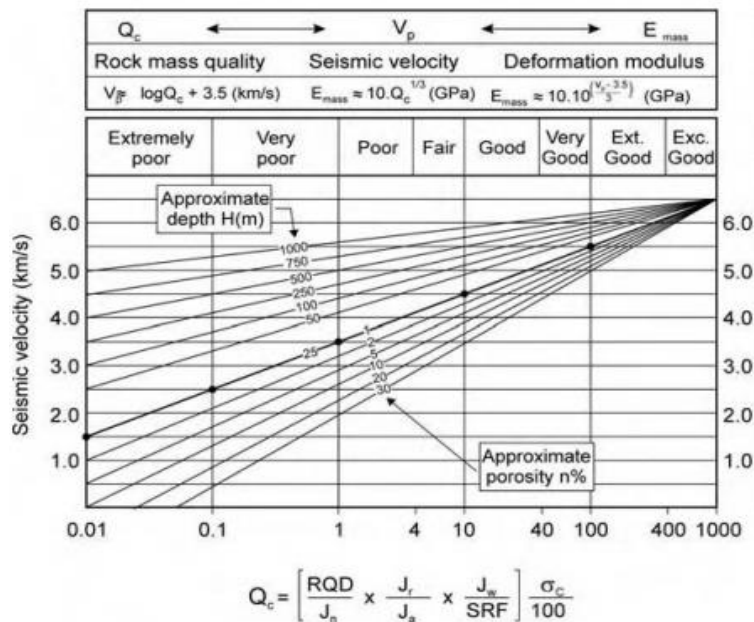


Figure 6: Integration of rock quality Q-VP-Emass in a model that incorporates depth, porosity and rock strength adjustments (Barton, 1995).

Seismic refraction method

These anisotropies possess important relations to elastic wave velocity, strength moduli, permeability, and deformation and so on. Elastic waves i.e. P-wave and S-wave are useful indicators to reveal those directional variances. In fact, propagation of these waves enlightens the subsurface below us. The way to investigate the subsurface using elastic waves is popularly known as seismic methods. This site exploration method is divided into two branches: Seismic reflection method and Seismic refraction method.

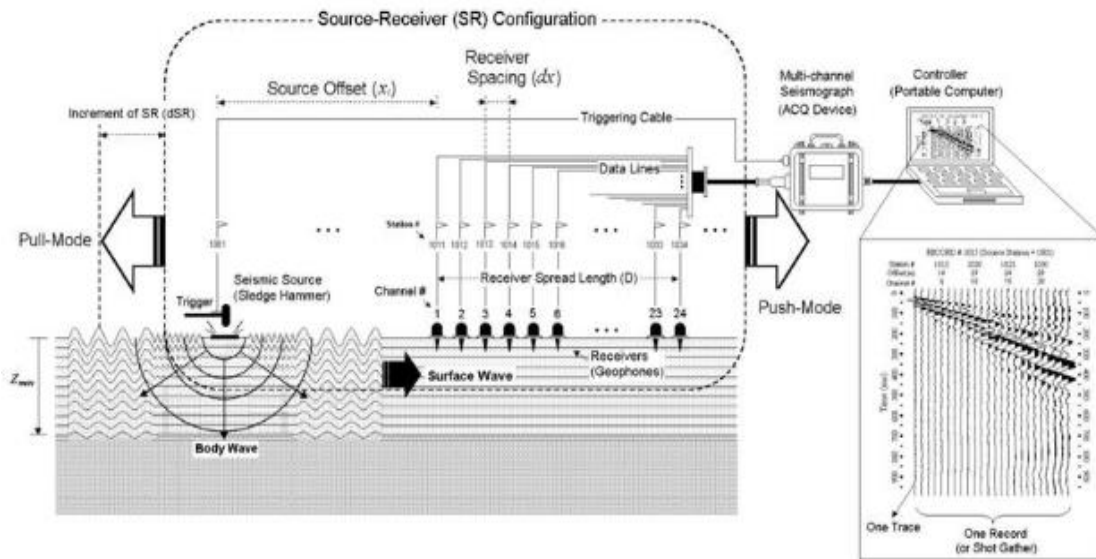


Figure 7: Basic components of a seismic refraction survey (Park Seismic, LLC).

The above figure describes the summary of the seismic refraction method. The major components are an energy source, geophones, a multi-channel seismograph, seismic cables to connect geophones and source to the seismograph, a laptop to show seismogram is connected to the seismograph. The energy source can be either hammer, air gun or explosive which generates elastic energy propagating through the subsurface and gets received by geophones. Geophones are installed in a predefined array depending on the aim of the survey. The frequency of them is

typically low (~14Hz) in this survey. This elastic energy consists of two types of waves: Body waves and Surface waves. Surface waves are slower and attenuate faster than the body waves. Body waves consist of two different waves: P-wave and S-wave. P wave travels by consecutive compression and expansion within the medium, wave propagation and particle vibration are in the same direction. While S-wave propagates by vibrating particles normal to the direction of propagation within the medium.

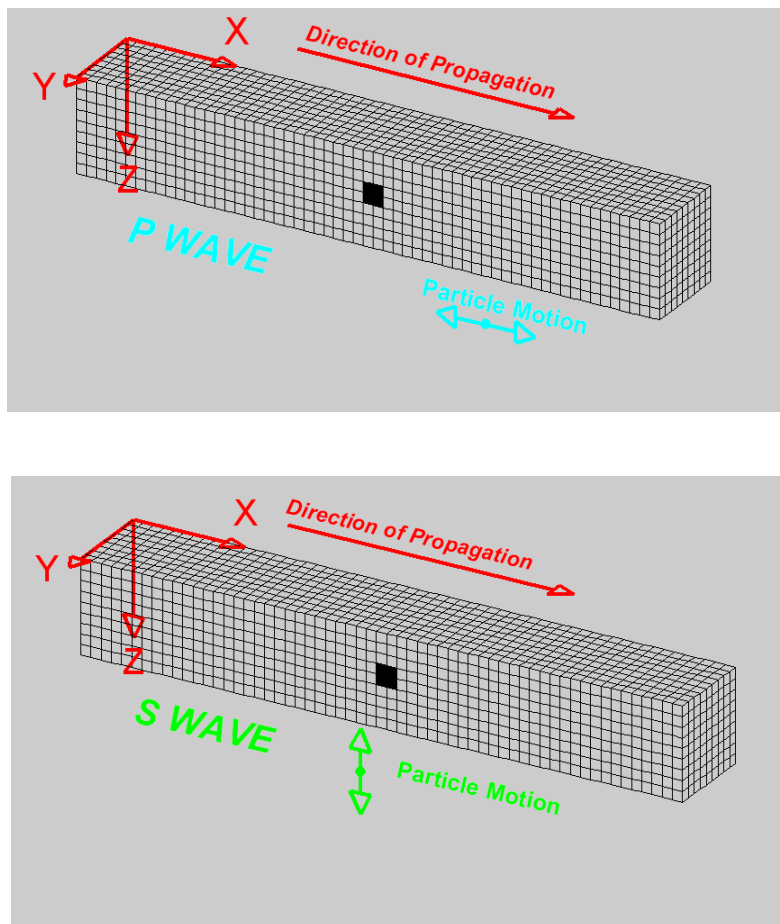


Figure 8: Body waves propagation and particle vibration (top: P-wave, bottom: S-wave) (Braille, 2010).

P-wave can travel through any medium except vacuum while S-wave travels through only solid medium. Their propagation depends on the bulk and shear modulus (Young's modulus and

Poisson's ratio) and the density of the medium. As fluid has no shear strength, so, S-wave cannot travel through it. The displacement of S-waves can have any direction in a plane normal to the direction of propagation and is therefore normally divided into a vertically polarized component (SV) and a horizontally polarized component (SH). P-wave travels faster than S-wave and the following table shows the ratio of two body waves for different rock types:

Table 2: V_S/V_P for different rock types (Burger, Sheehan & Jones, 2006).

Rock Types	V_S/V_P
Crystalline rocks	0.6
Sedimentary rocks	0.5
Soil and unconsolidated materials	0.4

Body waves (i.e. P- and S-waves) are the only wave types present within a continuous unbounded medium. In a medium with a free surface Rayleigh waves which consist of both longitudinal and lateral particle displacement (i.e. P- and S-waves) may appear. During the passage of Rayleigh wave, particles move along retrograde ellipses in the plane parallel to the direction of propagation. Its velocity is lower than the body waves. The amplitude of Rayleigh waves decreases quickly as it travels into the solids; The amplitude is maximum at a depth of 0.2-0.6 of the wavelengths and is almost zero at depth equal to the 1.3 of the wavelengths. This means Rayleigh wave cannot propagate through the solids. Another surface wave called Love waves appear within a thin layer having a density and elasticity that differs from the main medium

(Eitzenberger, 2012). In case of Love wave particle motion is alternating transverse motion that means motion is horizontal and perpendicular to the direction of propagation (Braile, 2010).

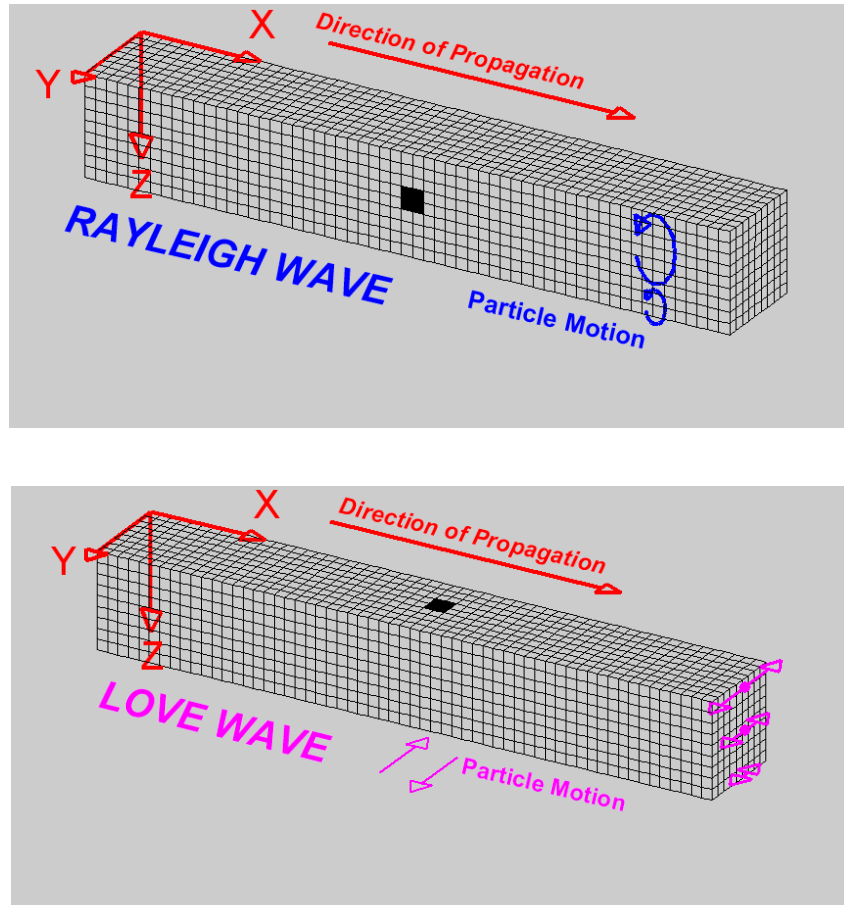


Figure 9: Surface waves propagation and particle vibration (top: Rayleigh-wave, bottom: Love-wave) (Braile, 2010).

Geophones nearer to the source, receive P waves directly from the source and these signals are known as direct wave. Some P-waves propagate through the subsurface, refracted by another velocity layer and travel back to the geophones away from the source as head waves. All the arrivals are displayed in the seismogram. The data analyst looks for the first arrivals in the seismogram and inverts these data to produce a velocity-depth model of the subsurface. The basic assumption of the seismic refraction method is velocity increases with depth. Seismic refraction is

aiming for locating bedrock, i.e. depth of backfill and landfill, details of subsurface and the target depth is around several tens of meters. The traveltime of the seismic wave depends on the acoustic properties of the subsurface materials which is a product of density and velocity of the material.

Seismic wave propagation through rock mass

The propagation of seismic waves through intact rocks depends on material properties of rock such as mineral content, grain size and shape, pores and micro-cracks. The waves follow both Huygens's and Fermat's principle during its propagation through a medium. Like other energy propagation, seismic waves attenuate as it travels through a medium. If there is no pores or cracks, two different types of attenuation take place: geometrical and material attenuation. Geometrical attenuation is the loss of energy due to expansion of wave front. In this type attenuation, the energy at a certain distance 'x' is inversely proportional to the square of that distance (Burger, Sheehan & Jones, 2006). Material properties of medium and frequency of the wave have no influence on geometrical attenuation.

$$Energy \propto \frac{1}{x^2} \quad 5$$

Material attenuation is the energy loss due to mechanical distortion (straining) of the material and partial transfer of energy into heat during wave passage (Burger, Sheehan & Jones, 2006). It is a non-conservative process and energy loss depends on the frequency of the wave and material composition, size and shape of grain. The loss is defined by the following equation (Burger, Sheehan and Jones, 2006),

$$I = I_0 e^{-qr} \quad 6$$

Here, I = Intensity at a distance r , I_0 = Intensity at the source, r = Distance traveled by the energy and q = Absorption coefficient (dB/λ) which has a proportional relation with frequency. Seismic waves with high frequency attenuate faster i.e. earth filters out higher frequency pulses as wave travels through it. So, earth can be considered as a low-pass filter.

Another type of attenuation occurs at the interface of two layers having different seismic impedance (product of density and velocity). At the interface, the partition of incident wave energy and amplitude occurs among reflected and refracted P and S-waves.

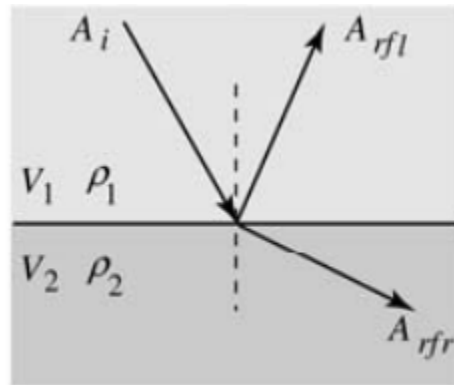


Figure 10: Partitioning of wave energy among reflected and refracted P and S-waves (Burger, Sheehan & Jones, 2006).

Here, A_i , A_{rfl} and A_{rfr} are the amplitude of the incident wave, reflected wave and refracted wave respectively. V and ρ are the velocity and density respectively, and 1 and 2 denote the first and second layer. Incident of P-wave and SV-wave produce the both reflected and refracted P-wave and SV-wave whereas incident of SH-wave only produces reflected and refracted SH-wave. The partitioned amount of energy can be computed by a set of equations (Zoeppritz, 1919). Assume a plane P-wave with amplitude A_0 incident on the boundary between two solid media. So, there will be both reflection and refraction and both P and S-wave will be produced by the course

of these two incidents. So, finally we will have four different waves: reflected P and S-wave, and refracted P and S-wave.

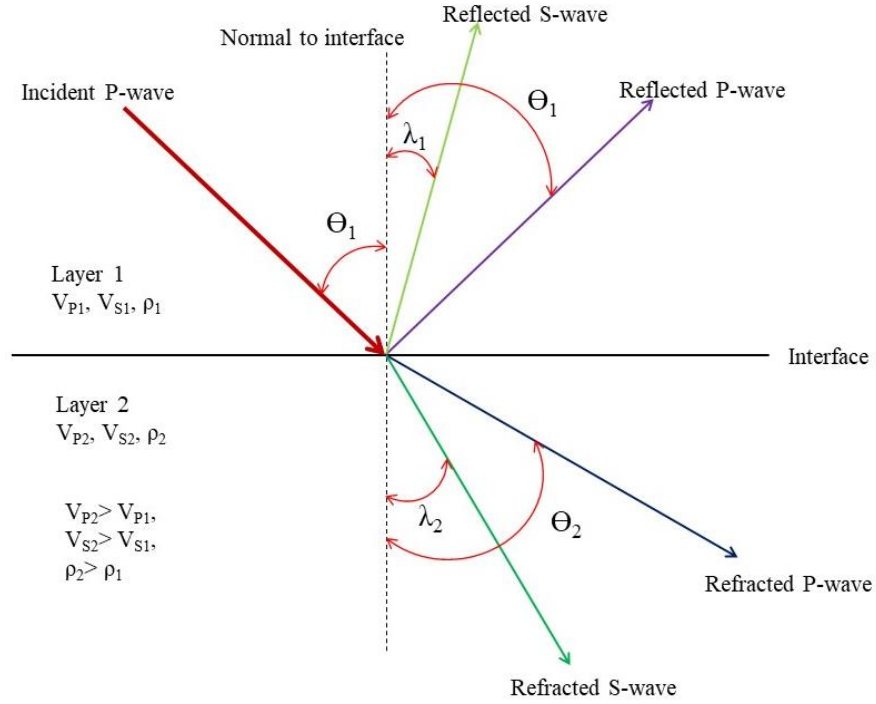


Figure 11: Partitioning incident of P wave (Image by author).

The amplitude of four resulted waves can be computed by following equations (Zoeppritz, 1919).

$$A_1 \cos \theta_1 - B_1 \sin \lambda_1 + A_2 \cos \theta_2 + B_2 \sin \lambda_2 = A_0 \cos \theta_1 \quad 7$$

$$A_1 \sin \theta_1 + B_1 \cos \lambda_1 - A_2 \sin \theta_2 + B_2 \cos \lambda_2 = -A_0 \sin \theta_1 \quad 8$$

$$A_1 Z_1 \cos 2\lambda_1 - B_1 W_1 \sin 2\lambda_1 - A_2 Z_2 \cos 2\lambda_2 - B_2 W_2 \sin 2\lambda_2 = -A_0 Z_1 \cos 2\lambda_1 \quad 9$$

$$B_1 W_1 \cos 2\lambda_1 + A_1 \gamma_1 W_1 \sin 2\theta_1 - B_2 W_2 \cos 2\lambda_2 + A_2 \gamma_2 W_2 \sin 2\theta_2 = A_0 \gamma_1 W_1 \sin 2\theta_1 \quad 10$$

Here, A_0 , A_1 , A_2 , B_1 and B_2 are the amplitude of the incident wave, reflected P-wave, refracted P-wave, reflected S-wave and refracted S-wave respectively. Θ_1 and Θ_2 are the angle of reflection and refraction for P-wave and λ_1 and λ_2 are the angle of reflection and refraction of S-wave. B , Z and γ are defined by the following equations,

$$\gamma_i = \frac{V_{Si}}{V_{Pi}} \quad 11$$

$$Z_i = V_{Pi} \times \rho_i \quad 12$$

$$W_i = V_{Si} \times \rho_i \quad 13$$

Where, $i = 1$ and 2

Solving the equations 7, 8, 9 and 10, the amplitude of the resulted waves can be easily computed.

Nowadays, the seismic refraction method is gaining popularity among geophysicists and geotechnical engineers because of its non-destructive, rapid and cost-effective nature. Users can produce a 3D tomogram if the data volume is sufficient. This method gives an overall image of the subsurface, whereas boring is expensive and gives only localized data. In addition, terrain conditions may not be advantageous for drilling. Within the first 50-100m of the subsurface, both vertical and horizontal velocity gradients vary rapidly and randomly due to the extremely variable nature of the soil cover. Considering these site constraints, the seismic refraction method is advantageous when compared to other exploration methods.

Regional structural pattern

The Black Warrior Basin, a foreland basin of the Ouachita fold-thrust belt, is bounded to the North by the Nashville Dome, Southeast by the Appalachian Mountains, Southwest by the Ouachita thrust front and on the West by the Reelfoot Rift (Arsdale, 2009).

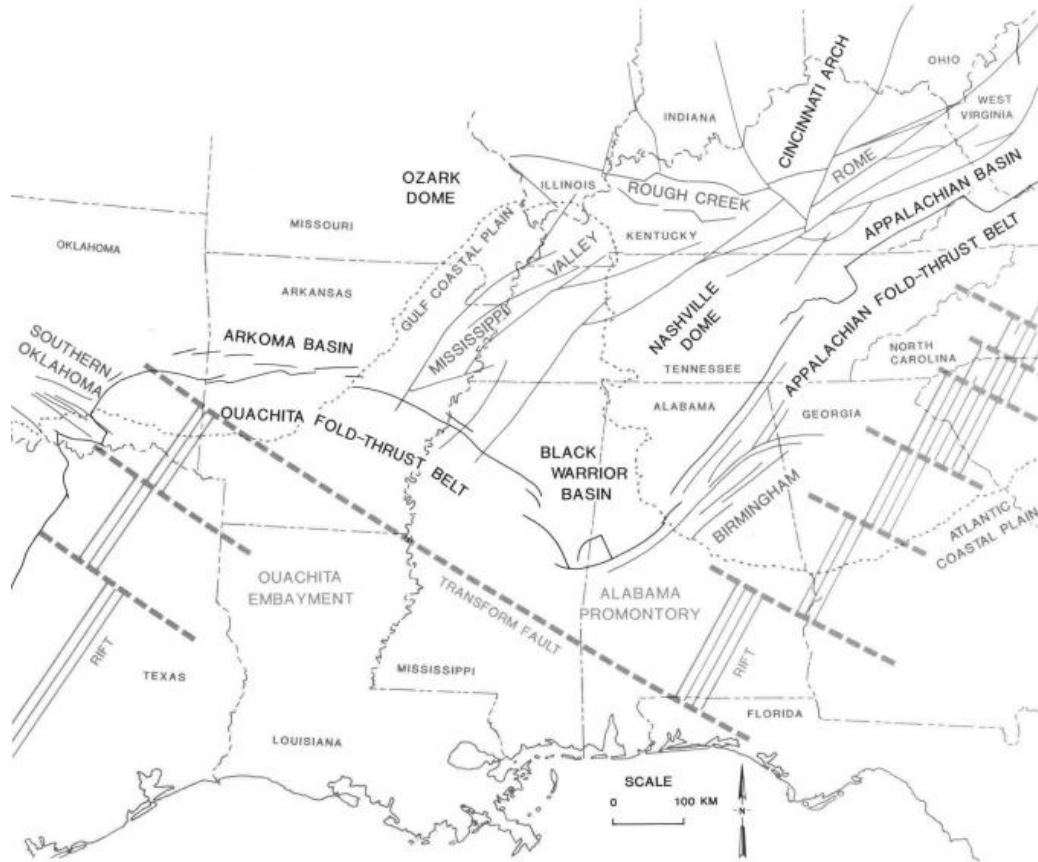


Figure 12: Outline of regional structural setting of Black Warrior basin (Thomas & Sloss, 1988).

This was formed tectonically and is the center of Pennsylvanian coal deposition in Alabama and the oldest sedimentary rocks of Mississippi have been found in this basin and ranged from Precambrian (granitic) to Pennsylvanian in age (Dockery III & Thompson, 2016; Lacefield, 2000). The Black Warrior Basin was south of the North American shoreline for much of the late Precambrian and Paleozoic time until it was filled by thick Pennsylvanian deltaic deposition during

the early part of the Appalachian Orogen (Lacefield, 2000). The geologic formations (Fm.) filling the basin are, in ascending order: Chilhowee Fm., Rome Fm. and Conasauga Fm. (Cambrian); Knox Dolomite (later Cambrian and Early Ordovician), Chickamauga Limestones (Middle Ordovician), Patterson Sandstone (Silurian-Ordovician boundary), Wayne and Brownsport groups (Silurian), Penters Chert (Devonian), Chattanooga Shale (Late Devonian) and Maury Shale, Mississippian Fort Payne and Tusculum Limestone (Early Mississippian) (Pike, 1968; Arsdale, 2009). This basin was a continental shelf in Cambrian through Early Mississippian and this environment ended with the deposition of the Floyd-Parkwood shale and sandstone succession and formation of major normal faults to the south during the Pennsylvanian (Arsdale, 2009). During the Late Carboniferous period, 3200m of the Pottsville Fm. (Ouachita and Appalachian Orogenies), was deposited as a sequence of alternating sandstone and shale into the basin and the Pennsylvanian Atoka Fm. is the youngest unit. Both of these formations have been thrust-faulted northward (Arsdale, 2009). After the Cumberland Plateau was uplifted, between 20,000 to 30,000 feet of Pennsylvanian sedimentary rock may have been eroded away during the Late Pennsylvanian and Permian and the remaining thousands of feet sediments formed the world's second thickest basin (Lacefield, 2000). Prior to erosion, the massive weight of the sediment and earthquakes caused a large section of the basin to subside and filled the lowland coastal swamps with sea water and dark, marine mud (Lacefield, 2000). The combined effects of subsidence, compaction of soggy sediment, and on-going deposition from the young and rapidly eroded Appalachians helped the landscape of the Black Warrior Basin achieving an equilibrium with the sea (Lacefield, 2000). Reverse faults may represent compressional features related to the larger tensional forces that produces the normal faulting and most of the faults in this area have been mapped in Pottsville Fm. (Rheams & Kidd, 1982). The dominant orientation of the strata in the

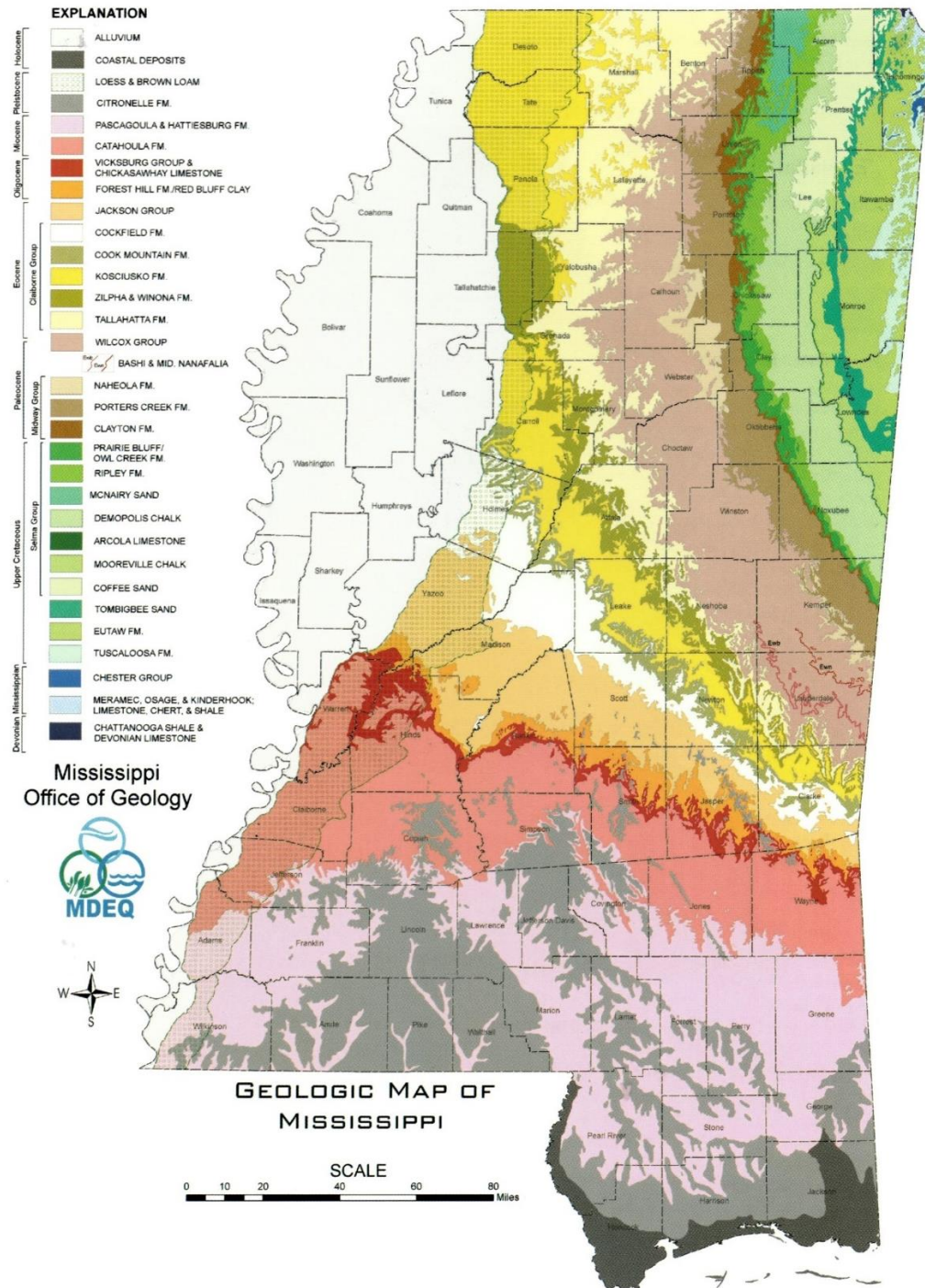


Figure 13: The geologic map of Mississippi (Dockery III & Thompson, 2016).

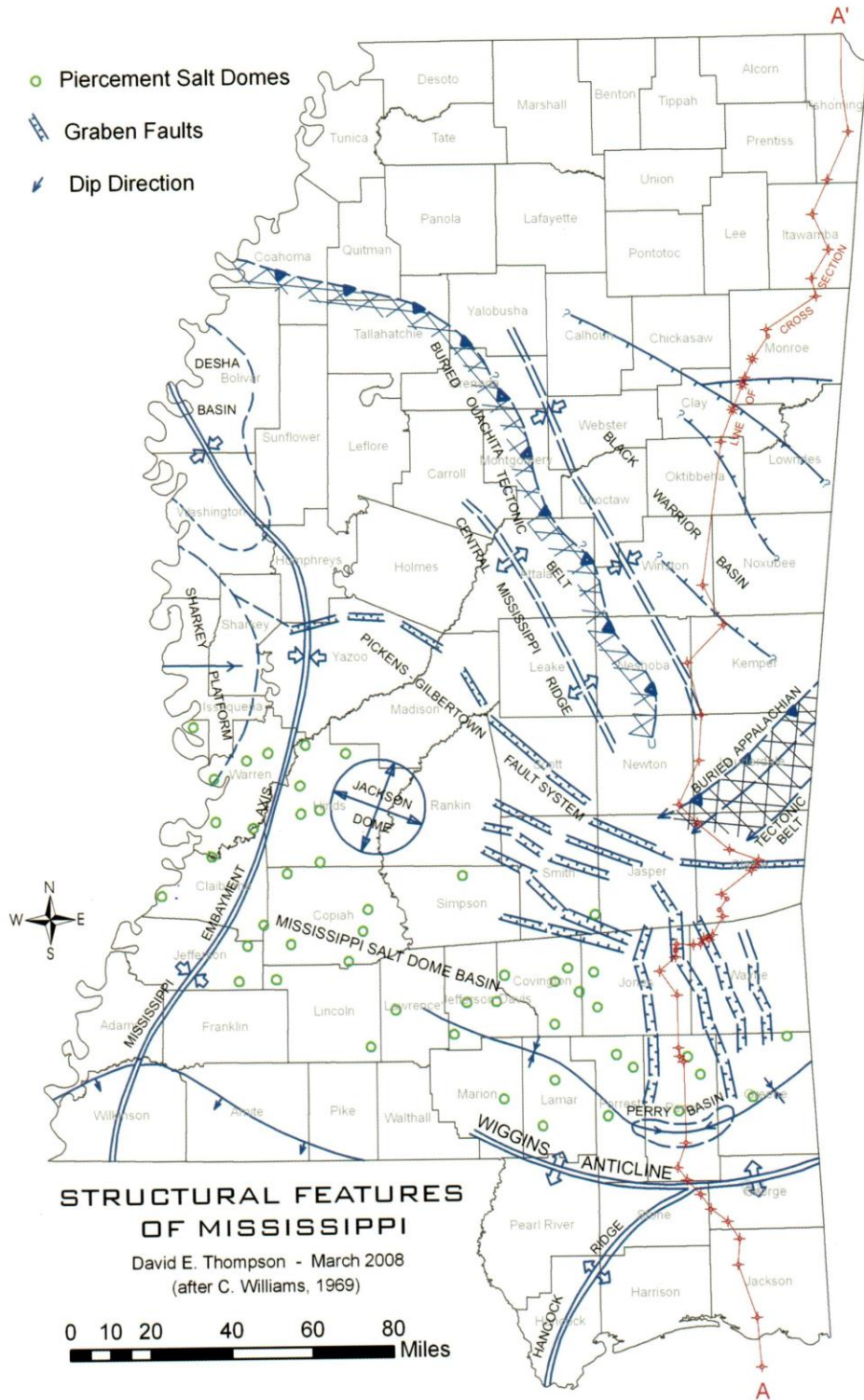


Figure 14: Structural features of Mississippi (Dockery III & Thompson, 2016).

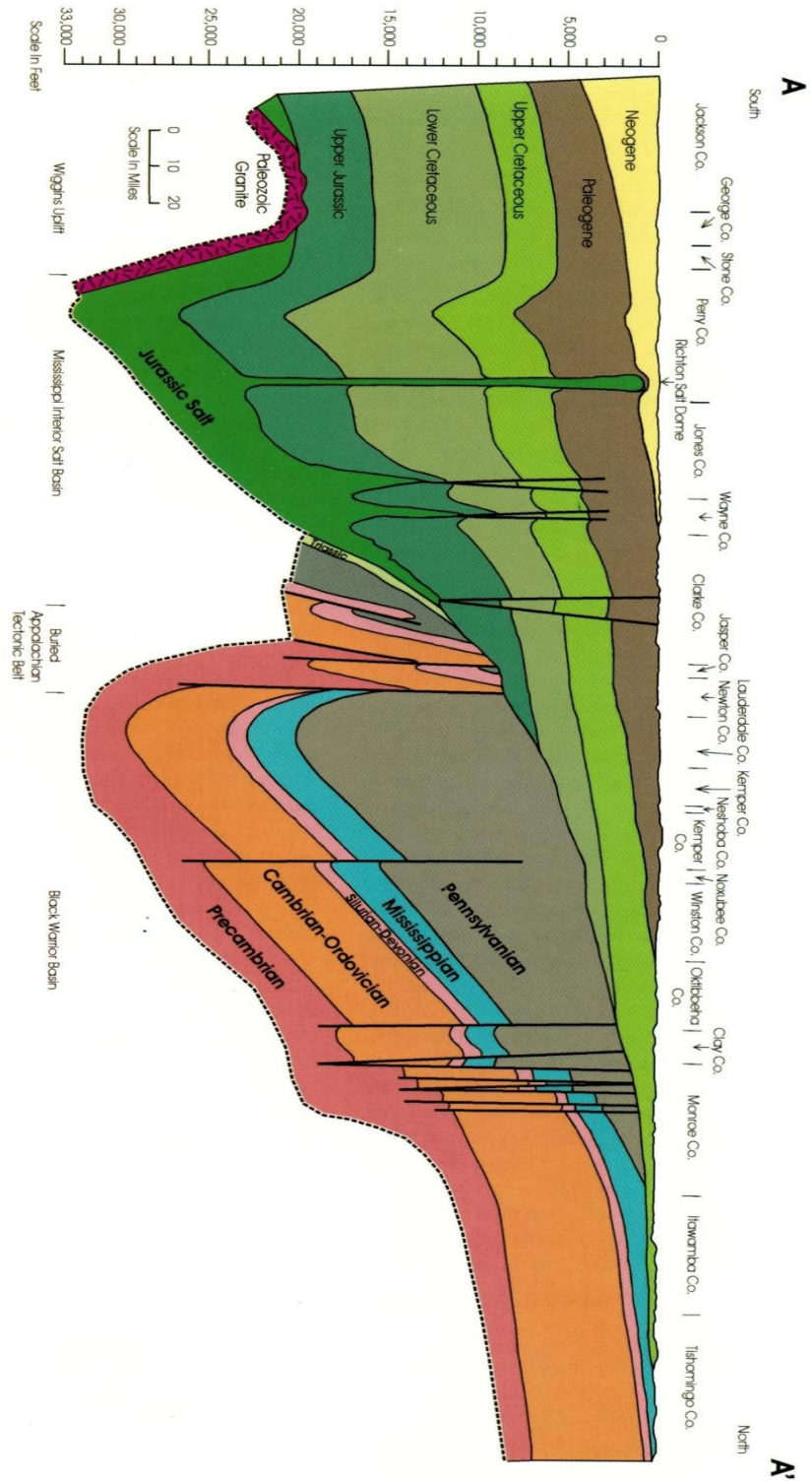


Figure 15: North-south cross section A-A' from the Mississippi-Tennessee state line to Horn Island in the Gulf of Mexico (Dockery III & Thompson, 2016).

Black Warrior Basin is NW-SE with an average dip of 60°-70° (Pike & Warren, 1968). However, these anomalies are not observed in the overlying post-Paleozoic deposition and these fault patterns are related to the post-depositional basin deformation (Pike & Warren, 1968).

The exposed Ouachita and Appalachian fold and thrust belts border the Arkoma and the Black Warrior Basin along the southern part of the North American craton (Hatcher Jr., Thomas & Viele, 1989). The Black Warrior Basin beneath the coastal plain has a triangular shape, limited on the southwest by the Ouachita orogenic belt and on the southeast by the Appalachian orogenic belt (Mellen, 1947). The Central Mississippi Uplift is a fold-thrust belt related to the Appalachians that has been displaced northward over rocks of Black Warrior Basin (Thomas, 1972, 1973, 1985a). The Black Warrior basin homocline has an average dip of less than 2° towards southwest. This homocline has been displaced by a northwestward normal fault system by 4km. On the southwest, this fault system intersects the front of the Appalachian fold-thrust belt at around 90° and extends northwestward entirely across the Black Warrior basin (Thomas & Sloss, 1988). The normal faulting is inferred to have been caused by a stress field with σ_3 oriented NE-SW direction (perpendicular to the normal fault strike), σ_1 vertical and σ_2 NW-SE. The extension direction is in the principle curvature direction for Ouachita related flexure and the fault appear to be part of a trend of Ouachita orogenic belt (Bradley & Kidd 1991; Cates et al. 2004). Both downdip gravity glide and flexural extension could have contributed to the stress state. Farther, west, along the Arkoma basin, this system of large-scale down-to-south normal fault extends beneath and approximately parallel to the frontal thrust faults of the Ouachitas. Frontal ramps in Ouachita thrust faults are positioned above these normal faults (Buchanan & Johnson, 1968). In case of Appalachian fold system, the main folding event postdates Pottsville deposition and small amounts of crystal-plastic grain deformation, including the cements, are widespread in this deposition (Wu

& Groshong, 1991). Twin strain measurements in Mississippian limestone indicate the maximum shortening direction is at a low angle to bedding and perpendicular to the fold axis indicating that σ_1 was oriented NW-SE (Cherry, 1990). The complete fold, fault and joint pattern could have been caused by a triaxial stress field with σ_1 oriented NW-SE horizontal (perpendicular to fold trend), σ_3 oriented NE-SW- horizontal (parallel to fold trend), and σ_2 vertical (Groshong Jr. et al., 2009).

Literature review

Most of the work on identifying rock mass anisotropy took place in the lab. Velocity anisotropy due to the foliation, cleavage and the schistosity was identified on orthotropic slate (Duellmann & Heitfeld, 1978; Tsidzi, 1997). Smooth transition in velocity nicely followed the rotation of samples and velocity hysteresis on the unloading section was presumed as fabric damage or micro-cracks formation due to loading.

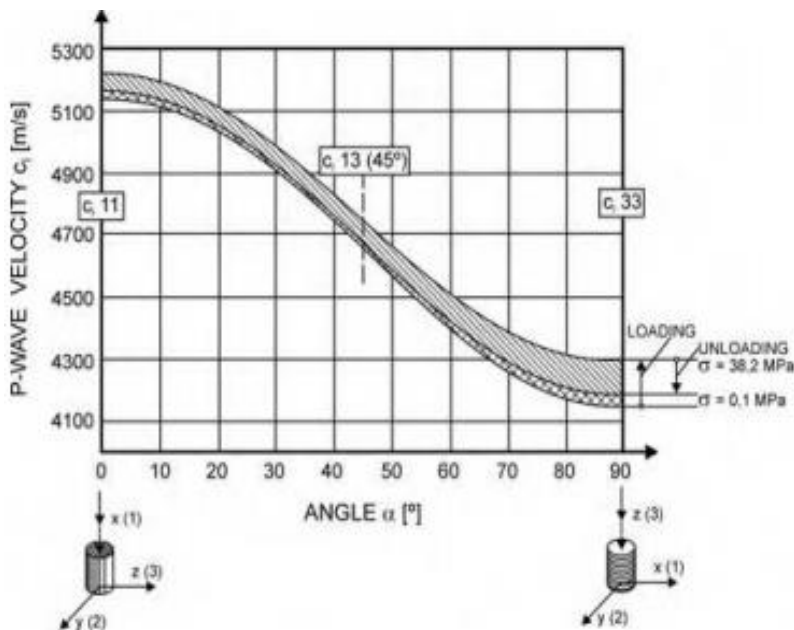


Figure 16: Velocity anisotropy of slate due to cleavage (Duellmann & Heitfeld, 1978).

In the above figure, α is the angle between the P-wave velocity and cleavage in slate. Ultrasonic pulse velocity test showed similar results like seismic wave (Tsidzi, 1997). The summary of this work is presented in the Table (2). For all kinds of foliated rocks, ultrasonic velocity is the highest along the foliation and least normal to foliation. This is valid for saturated and dry samples. Usually, anisotropy is small for fine-grained samples and large for coarse-grained. However, the saturation increases the anisotropy in fine-grained samples and decreases in the coarse-grained samples. Here, β is the angle between the wave propagation and foliation.

Table 3: Effect of foliation, cleavage, and schistosity on V_P . Both dry and saturated state (Tsidzi, 1997).

Rock Type	$\beta=0^\circ$	$\beta= 45^\circ$	$\beta= 90^\circ$	$\beta= 0^\circ$	$\beta= 45^\circ$	$\beta= 90^\circ$
Condition	Dry	Dry	Dry	Saturated	Saturated	Saturated
Gneiss (SW)	5102	4211	3956	5918	5237	5081
Phyllite (F)	6010	5130	5090	6050	5417	5307
Schist (SW)	6641	5802	5151	6706	5932	5378
Slate (F)	5913	5074	4893	5746	4722	4283

A crack tensor technique was developed which was consistent with the laboratory experiment and in site tests on granite sites (Oda, Yamabe, & Kamemura, 1986). Laboratory samples were prepared by plaster with deformable grease paper that acted as cracks. The squared V/V_0 ratio was normalized by intact sample velocity V_0 . Samples with almost aligned cracks showed velocity anisotropy whereas samples with randomly oriented cracks showed an isotropic reduction of velocity Figure (17(i)). Similar results were observed on granite sites Figure (17(ii)).

Their crack tensor showed remarkable agreement with the seismic survey and velocity distributions followed major joint sets direction.

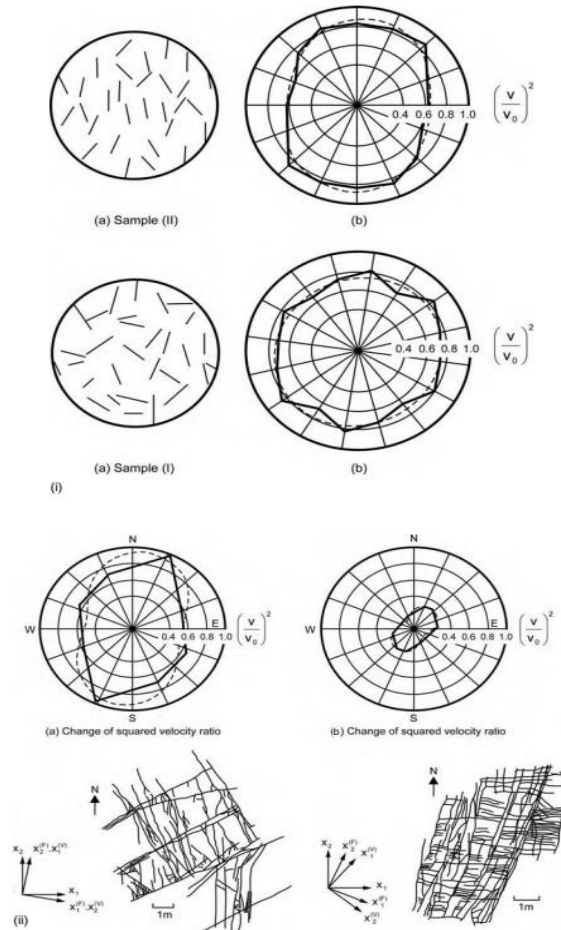


Figure 17: Velocity anisotropy with gypsum samples with deformable cracks and two jointed granite sites in Japan (Oda et al., 1986).

An exclusive experiment was conducted to show the directional dependence of seismic velocity under uni-axial pressure (Nur, 1971). The following figure was the summary of his experiment. Velocity increase is greater along the stress direction rather than normal to it. Because cracks perpendicular to the stress close due to applied pressure while open further along the stress direction.

This fairly represents in situ velocity anisotropy effects since horizontal σ_{\max} has a trend to be parallel or sub-parallel to major jointing; so, velocity along the joints is highest.

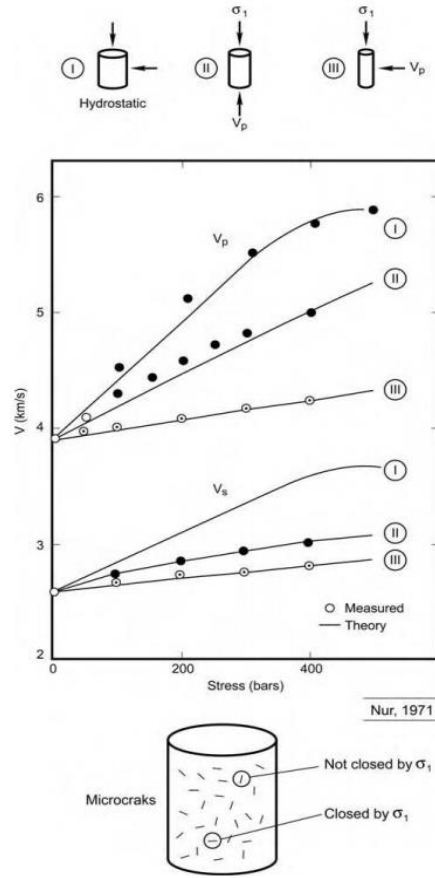


Figure 18: sensitivity of the velocity anisotropy towards uniaxial loading (Nur, 1971).

(I: hydrostatic, II: measured parallel to the uniaxial, III: measured perpendicular to the uniaxial)

Seismic refraction survey following a radial pattern (20° interval) was conducted at four sites in chalk in Lincolnshire, England (Nunn et al., 1983). Strong anisotropy was recorded on three sites (CFR, RGF and RGQ). Total velocity anisotropy $(V_{\max} - V_{\min}) / V_{\max} = 0.38$ which is $\pm 20\%$ around the mean velocity 2.25 km/s. The following equation shows relationship between the compressional wave velocity through rock mass with crack (V_{po}) and without crack (V_p).

For dry cracks:

$$V_p^2 = V_{po}^2 \left(1 - \frac{71}{21\varepsilon} - \frac{8}{3\varepsilon} \cos 2\theta + \frac{\varepsilon}{21} \cos 4\theta \right)$$

14

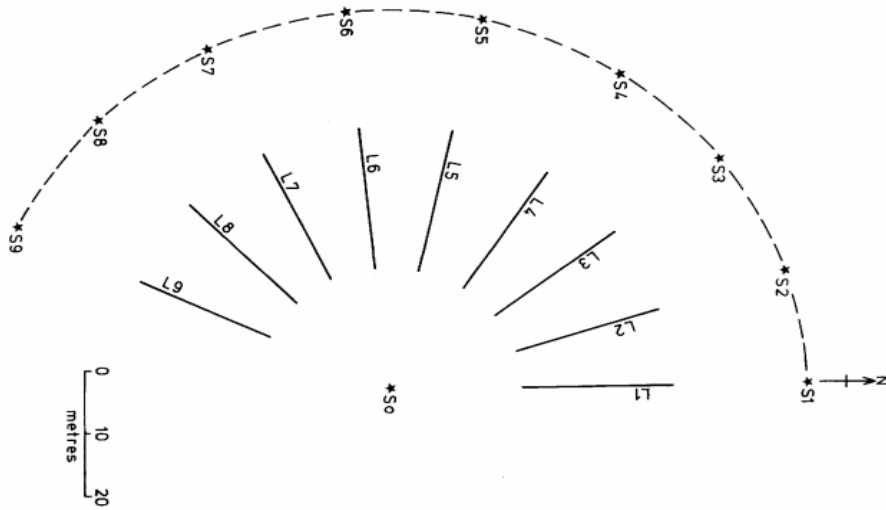


Figure 19: Seismic observation scheme showing geophone spread and source point arrangement e.g. solid line L7= Line 7 occupied by 12 geophones at 2m spacing and recorded from shot positions S0, S6, S7 and S8. 'Fan' arrangement (dashed line) of geophones at S1 to S9 were recorded from the source positions (Nunn et al., 1983).

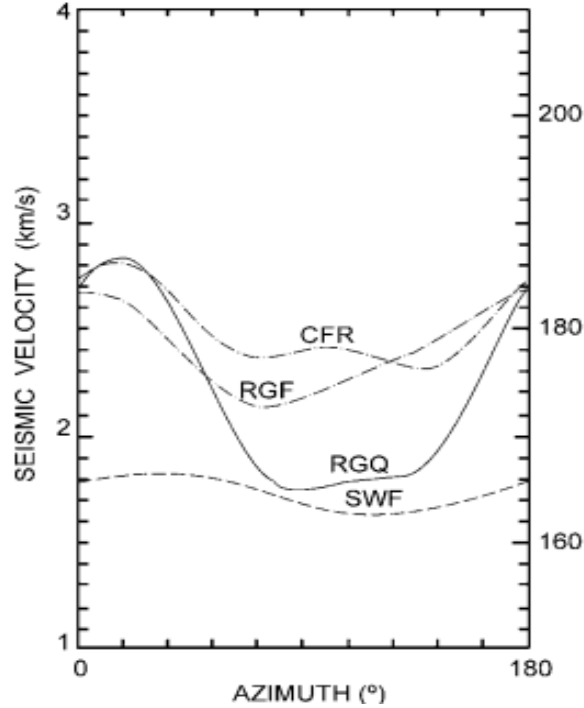


Figure 20: Azimuthal V_p anisotropy at jointed limestone sites in Lincolnshire, England (Nunn et al., 1983).

For saturated cracks:

$$V_p^2 = V_{p0}^2 (1 - 8/21\varepsilon + 8/21\varepsilon \cos 4\theta) \quad 15$$

In the above equation, crack density $\varepsilon = Nr^3/V$ is defined by the number of cracks 'N' in a volume 'V' with radius 'r'. ' θ ' is the angle of incidence relative to normal of crack plane. It is important to mention that the above equations did not account for the effect of stress on joint closure or seismic visibility. To differentiate the velocity anisotropy between closely and wider joints, seismic wave of wavelength 8-15m and ultra-sonic wave of wavelength 0.8-1.0m were used on dolomite at Ingouri Hydroelectric Station in Caucasus (Lykoshin et al. 1971). In figure 21, solid ellipse (ellipse a) represents the anisotropy of ultra-sonic velocity due to small scale joints. The length of ultra-sonic velocity is close to the distance between these joint systems, so, these waves

are influenced by the orientation of these joints. On the other hand, seismic velocity is more influenced by the large-scale joints systems (ellipse b), as the inter-joint distance there was comparable to seismic wave.

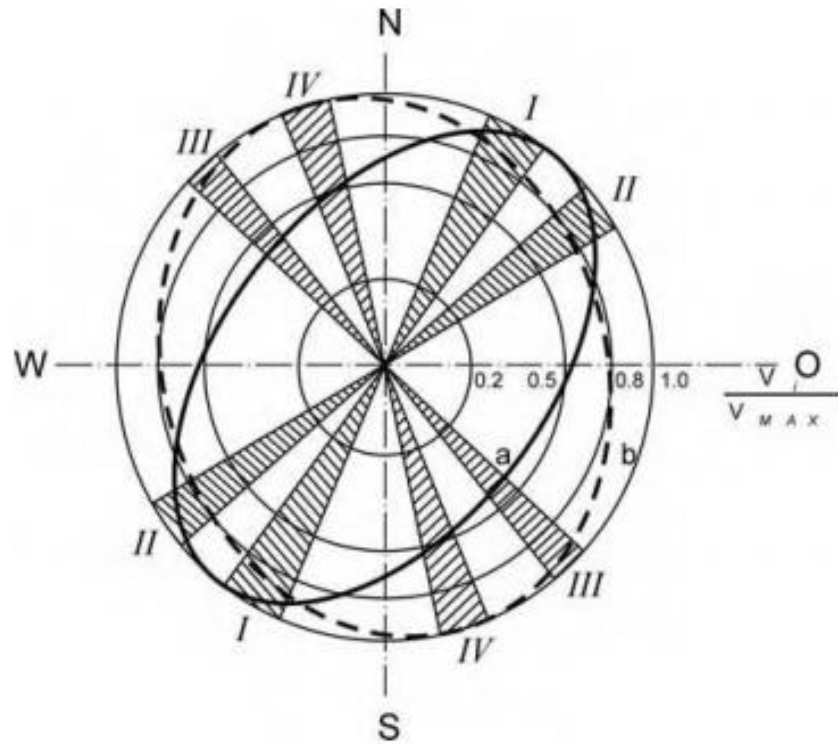


Figure 21: Change in velocity anisotropy for different frequencies of jointing (Lykoshin et al. 1971). (set I & II: closely spaced joints, set III & IV: wider joints).

CHAPTER 3

METHODOLOGY

Initial test of refraction tomography: Location

Early study with this software has been done on the Coldwater River Levee, Tunica, MS. That study was aimed to find out the geologic and structural structure of the levee and the longitudinal and lateral variation within the structure.

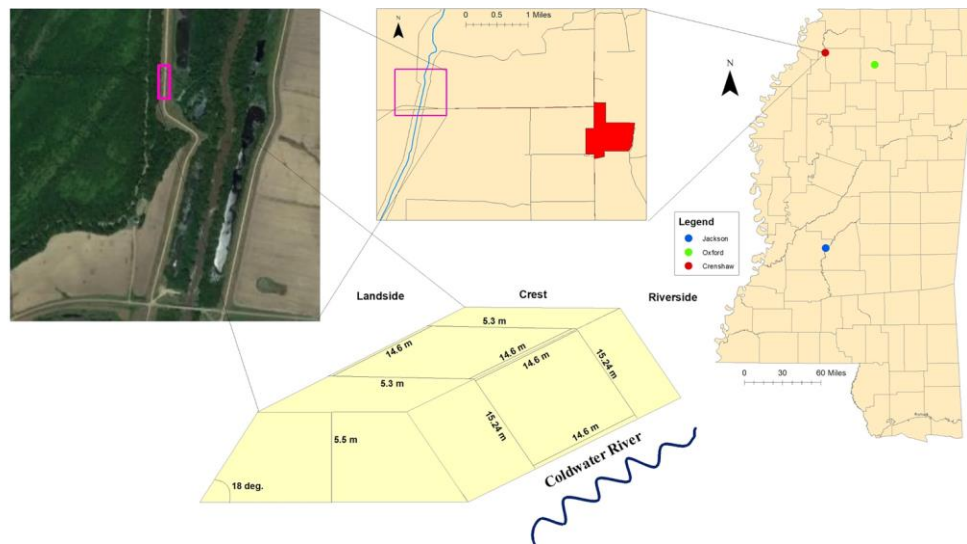


Figure 22: Location of the segment of levee at Tunica, Mississippi (Rhodes, 2018).

Geology

The test area was located along the west branch of the levee. The dominant soil is Shakely clay and Arakutla clay loam. In addition to this soil, transported material was used to build the levee. These soils are poorly drained (USDA, 2013) and have natural water content of about 29-

32% (in percent dry weight). The Coldwater River levee was built during the 1920s by the United States Army Corps of Engineers (USACE). The levee has been modified several times over the years, notably in the 1970s when they raised and widened the levee (USACE,1965). These modifications are the results of not only the needs of the time but also failures that occurred on the levee slope.

Study plan

The survey was conducted on both sides of levee: landside and riverside. The following diagram has illustrated the survey profile of this study. Three orange lines are showing the positions of seismic refraction survey profile and these lines are on the slope. There were an additional two profiles on the riverside: at the bottom of the slope and at the junction. Also, there was an additional profile on the landside which was at the bottom.

On each side, there were four profiles on the slope 3.81m apart except for the profile on the junction on riverside. The first profile on both sides was located 3.81m from the crest. The same geophysical instrument and software have been used in that study. Receivers were spread out along the profile at two feet spacing, and to get a good signal-to-noise ratio three shots stacking has been used. First, the raw data were imported to the Rayfract® directory. First arrivals were picked by interactive mode. Bidirectional filter and bandpass filter (4-24Hz and 8-20Hz) were used to reveal the signal from noisy traces. Later, a horizontally averaging initial (Wiechert-Herglotz method) model was prepared to get an artefact free initial model and then the tomogram was prepared by Wavepath Eikonal Traveltime (WET) method (Schuster, 1993).

Results and Discussions

There were five lines on the riverside and four lines on the landside of the levee. Figure: B1(1) was nearest the crest and the figure: B1(5) one was on the levee junction. First, one meter first four tomograms in figure: B1 represented the very loose material. We have observed vegetation on the riverside and due to vegetation, this low-velocity zone existed. Tomograms in (figure: B1(1) and figure: B1(2)) didn't reach the compact zone, (figure: B1(3) and figure: B1(4)) reached the compact zone and last tomogram (figure: B1(5)) reached the core of the levee. As we moved to the junction, the seismic waves had more chance to hit the core.

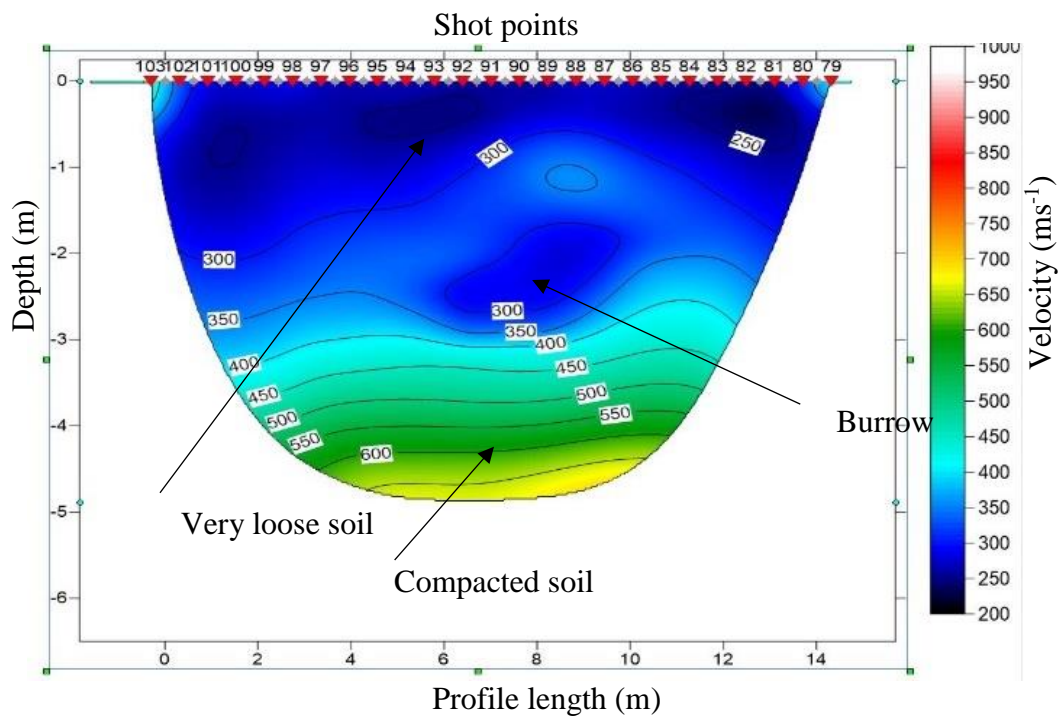


Figure 23: Sample diagram from initial study.

On the landside, figure: B2(1) was nearest to the crest and the figure: B2(4) one was on the bottom of the slope. All the tomograms showed a loose zone on the top couple of meters depth which is due to vegetation. Seismic waves hit the compact zone on the last tomogram (figure:

B2(4)). The saturated zone was deeper on the landside. In fact, on the landside this zone is below 6m from the surface, which is beyond the limit of our seismic profile.

Conclusions

- Both sides of the levee have the vegetation layer on the top, then a compact zone and finally the core of it.
- Figure: B2(3) showed a loose pocket at 2m depth. A burrow was identified in the field. Size and position of this loose zone matched with field observation.
- The saturated zone is deeper in the landside of the levee than that of in riverside.
- Besides the seismic refraction survey, GPR (ground penetrating radar) and ERT (electrical resistivity tomography) were applied along with the same profile. Combination of three different geophysical methods gave a better control on the subsurface features.

This seismic refraction analytical method works good on soil, though it did not show any anisotropy. But we have gathered experience on the software working on soil medium and apply this on my study area to have better control on it.

Conceptual design of study

The idea is the implementation of refraction tomography software to understand the subsurface without any drilling. To overcome the non-uniqueness characteristic of seismic survey, at least a cut-slope face is necessary to evaluate our results. Cut-slope must be analogous to outcrop containing the joint/joint sets which will be used to check the validity of our analysis and results. A road side-cut or a quarry would be an ideal place for this kind of data acquisition. As these two

kinds of places typically have large plane or less undulated surface to conduct refraction survey and vertical cut faces to support our hypothesis. The survey area may have soil covering or not.

For a hard surface or a surface where insertion of geophone into the ground may cause damage to it, use of clay mix or plaster is a good idea to keep these receivers in contact with the ground. The survey will follow a radial pattern to get the most accurate orientation of the joint sets.

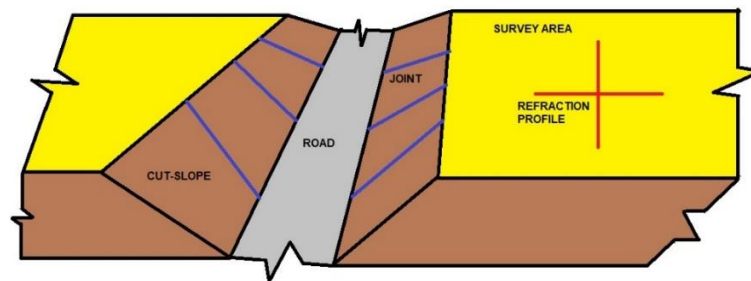


Figure 24: Schematic diagram hypothetical survey plan (Image by author).

This pattern must contain at least two perpendicular profiles; the higher the number is better but the maximum of six profile is enough to determine the anisotropy. The angle between each consecutive profile should be equal, which will help in interpretation. This pattern has proven to be useful in identifying the orientation of joint sets in the subsurface (Nunn et al., 1983). The velocity distribution in the refraction tomogram will tell us the direction of discontinuity. Least values of seismic velocity correspond to the wave propagation perpendicular to the discontinuity and the greatest value corresponds to the propagation direction parallel to the discontinuity. The analysis software Rayfract[®] has also some requirements for data acquisition. The shot location has to be at least at every second geophone location and end-shot should not be farther away from corresponding end geophones by more than three times the spacing. The site must have an outcrop to validate the results and may have a soil covering or have an exposed bedrock. Data is to be acquired by Geode, a single channel seismic refraction instrument and with its interface

Geometrics Seismodule Controller. The output data is SEG-2 formatted file (Pullan, 1990). Rayfract® uses first arrivals, picked either in an interactive or automatic way, to make a 1-D initial model. The initial model is based on basically Delta-t-V method (Gebrande & Miller, 1985). The user either can use this model or horizontally averaging Delta-t-V (Wiechert-Herglotz) model to produce a 2D tomographic image by WET Wavepath Eikonal Traveltime Inversion (Schuster, 1993). At the same time, a synthetic forward model is run to compute the misfit between user-defined and synthetic picks (Lecomte et al., 2000). After going through some trials and - errors, a reliable output is obtained.

Site selection: Study area 1

The first study area is a roadside area by US-62, Hardy, AR and an abandoned dolomite quarry by 119-1 Co Rd 165 Tishomingo, MS. In my observation, the rock mass in this area was mainly calcite. We have observed solution features through the rock slope which has been marked by red ellipses.

Site selection: Study area 2

The second study area was an abandoned dolomite quarry owned by Vulcan Materials Company. The site is located by 119-1 Co Rd 165 Tishomingo, Mississippi. The lake by the site is known as Providence Branch of Cripple Deer Creek. The total area is around 350 acres and our survey location is about 460ft above sea level. The bedrock is mainly dolomite with overburden backfill material.

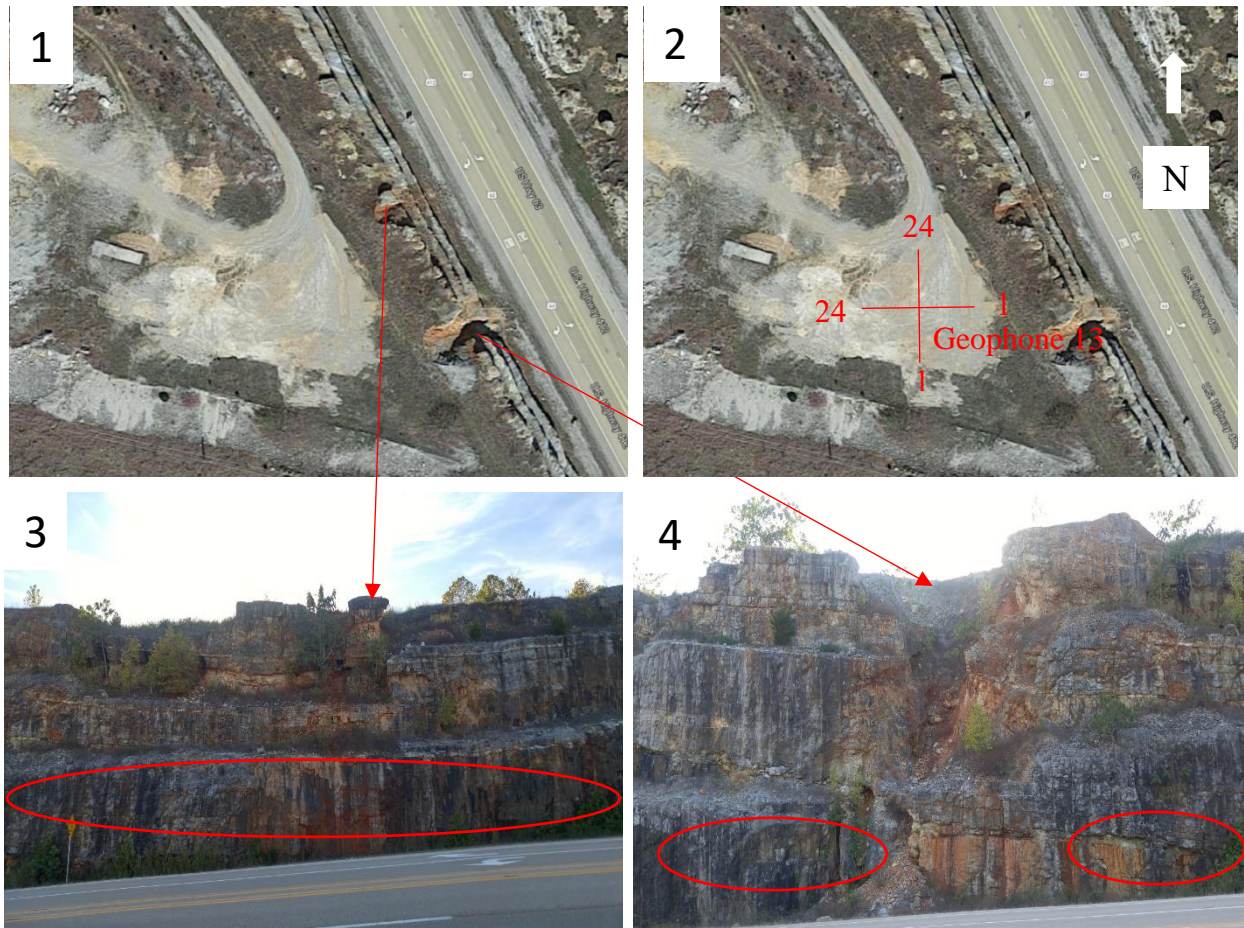


Figure 25: First study area. 1) Aerial view of the area, 2) Survey plan, 3 & 4) Field observation red elliptical boundary. The red arrows are indicating two features along the cut-face.

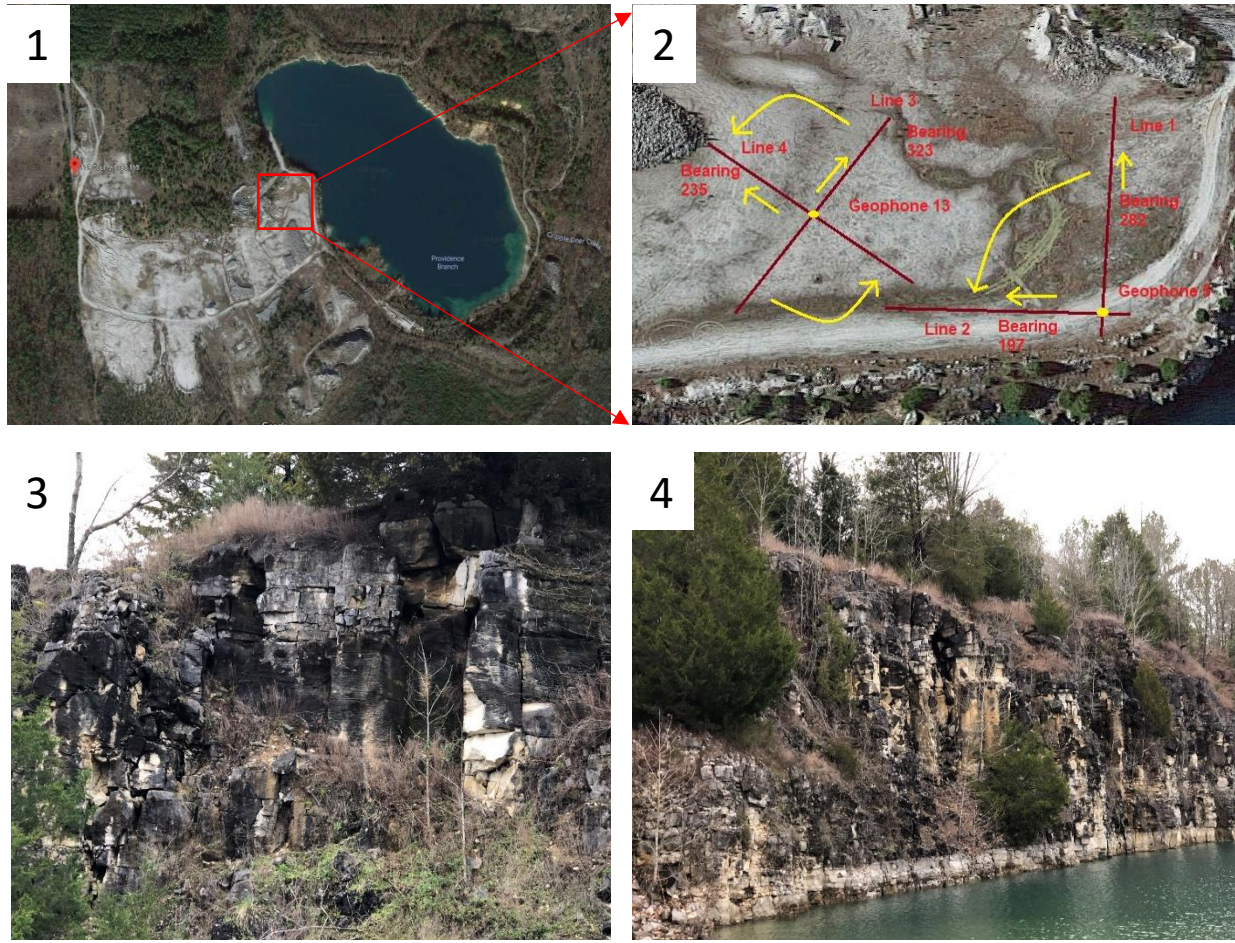


Figure 26: Second study area. 1) Aerial view of the area, 2) Survey plan and 3 & 4) Field observation.

Data collection

From the first area, data were collected in two orthogonal profiles which were the minimum requirement of our study on October, 23rd, 2018 (figure: 25). The surface was quite hard, hammer and nail have been used to penetrate geophones into the ground. In addition, clay mix has been

used to ensure a better coupling of geophones with the ground. The profiles intersected in the middle (13th geophone) and the bearing of them were 86° and 358°.

From the second area, the data was collected on February, 16th, 2019. Ground varied from hard to soft from place to place and was saturated from recent rainfall. Data was collected in two orthogonal lines in two pairs from this area (Figure: 26). The first pair intersected at 19th geophone and second pair intersected at 13th (middle) geophone. There is a lake formed by an abandoned pit beside the site. The bearing of the profiles of the first pair was 282° and 197° and for the second pair, it was 323° and 235°.

Here is the summary of our refraction survey.

- 1:24 Geometrics seismograph
- 14 Hz vertical component geophone
- Sledgehammer with impact trigger switch
- Geometrics seismodule controller for data acquisition
- Shot spacing: 2 ft (area 1), 2 m (area 2)
- Stacking option: 3 shots
- File type: SEG-2 (.dat format)

Seismic refraction data analysis software: Rayfract[®]

Typically, the seismic refraction software has three components:

- I. A tool to generate an initial model based on the first arrival picks,
- II. An inversion method for adjusting the velocity tomogram until an acceptable match between observed and calculated first arrival is achieved.
- III. Finally, a forward modeling algorithm to calculate the source-receiver traveltimes based on current velocity model.

In this study, Rayfract[®] has been used to analyze the raw data obtained from the field. This software uses DeltatV method to create an initial model (Gebrande & Miller, 1985). This method assumes subsurface has constant vertical velocity gradient model. This method determines layer bottom velocity from CMP sorted traveltimes curves by linear regression and the layer top velocity by Newton-Raphson root finding method which is made fail-safe by the inclusion of bisection method whenever Newton-Raphson does not work. To model the subsurface with a constant velocity model and enable the DeltatV to handle sudden velocity change Modified Dix inversion and Intercept Time inversion were incorporated with DeltatV (Winkelmann, 1998). Another means of producing an initial model is 'smooth inversion' which is basically a horizontally averaged DeltatV (Wiechert-Herglotz) model. The DeltatV initial model contains some artifacts which are carried to the final tomogram during inversion. The 'smooth inversion', on the other hand, offers an artefact free initial model. The software uses the WET (Wavepath eikonal traveltimes) inversion method to reduce the misfit between calculated and observed first arrival picks (Schuster & Quintus-Bosz, 1993). This method computes wavepath by using the finite difference solution of eikonal equation (Schuster, 1991). The forward modeling algorithm used to check the robustness of the final tomogram is the first order eikonal solver (Lecomte et al. 2000). This can handle any kind of geologic situation and topography of the surface. Finally, this software calls Surfer[®] to display the models.

Noise analysis

Noise is an inherent part of seismic signals. The notable sources of noises are: trees, winds, foot step, nearby electric line and vehicles movement. Signals received by distant geophones mostly get affected it. Its presence plays an important role in identifying the first arrivals. To

identify its nature, first the SEG-2 file has to be converted into ASCII file using the SEG-2 to ASCII decoder, which comes with the Geode.

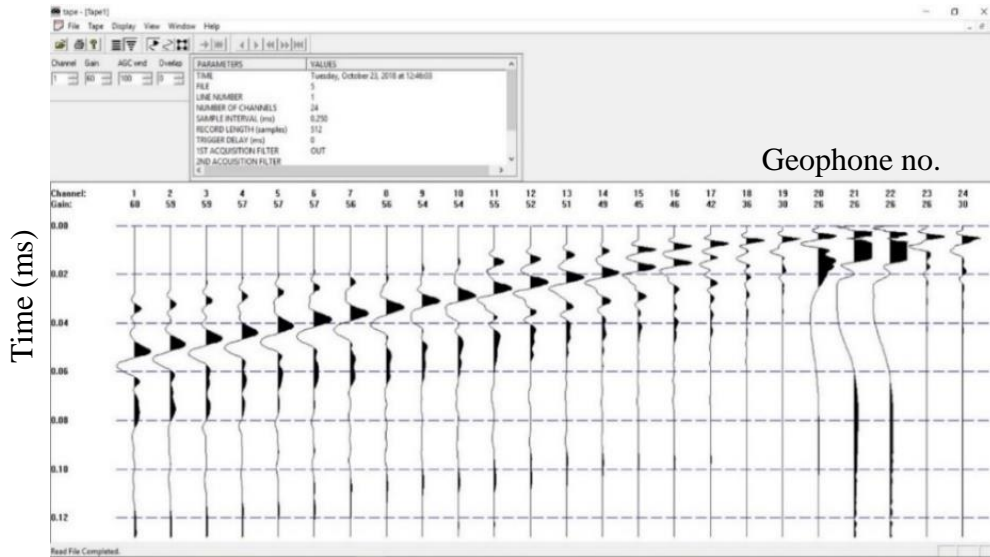


Figure 27: SEG-2 to ASCII Decoder.

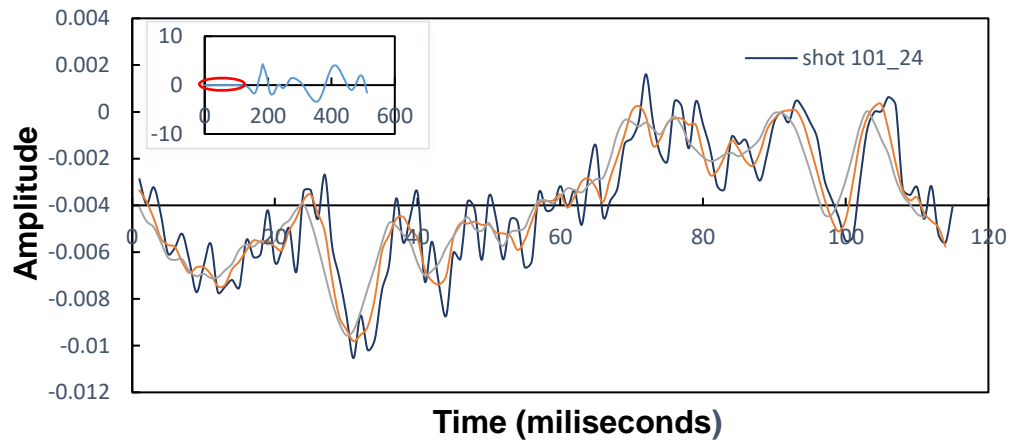


Figure 28: The apparent straight line in the seismic trace was not straight at all.

After decoding the desired traces (distant traces mostly) into ASCII, MS-Excel was used to plot the traces at trace scale and the noise part at noise scale. When the noise portion was isolated and plotted separately, it was surprising to see that the apparent straight line in the seismic traces

was not straight but rather a mixture of many high frequencies wave superimposed on a low-frequency sine wave. These hidden intricacies make first arrival pick difficult during the data analysis

CHAPTER 6

RESULTS

Velocity tomogram from the first study area

The unit along the X and Y-axis is meter and velocity has unit ms^{-1} . On the top of each tomogram the red dots denote the shot number. These units are valid for all the tomograms in this study. The first line is based on horizontally averaged DeltatV model and within 20 WET iterations, a reliable solution has been obtained. Wavewidth is 4.8% of central frequency 50Hz and RMS error is 1.2% (<2.0%).

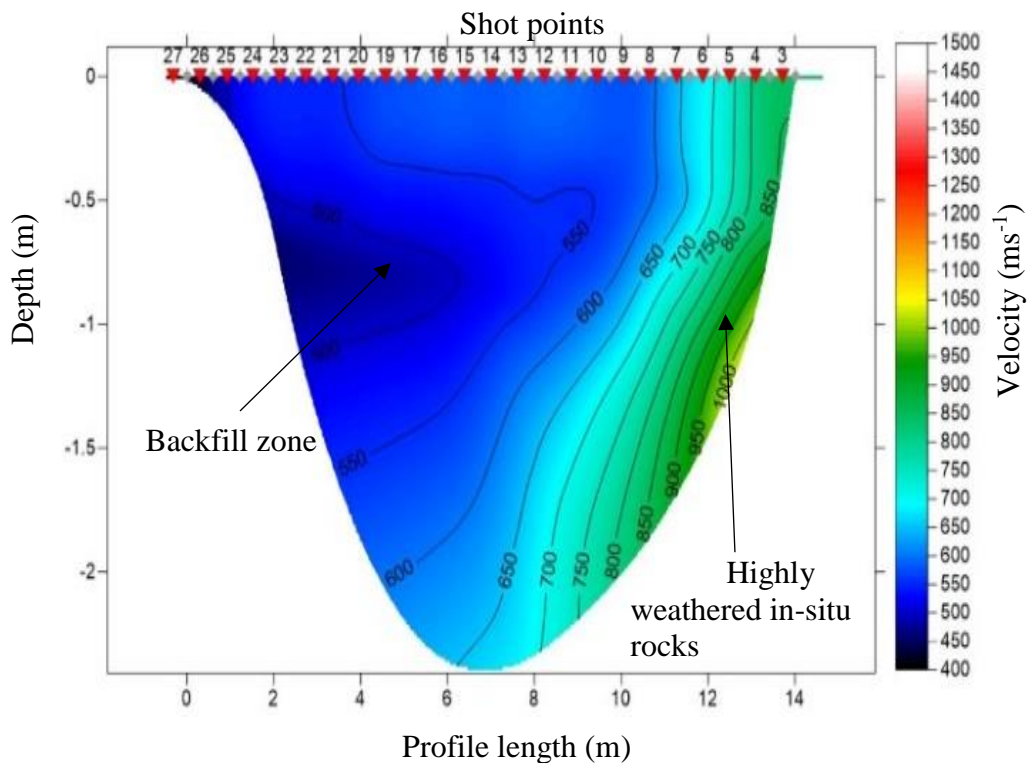


Figure 29: Study area 1 (Road cut site): Line 1 tomogram

The second line is based on DeltatV model and within 20 WET iterations, a reliable solution has been obtained. Wavewidth is 3.4% of central frequency 50Hz and RMS error is 1.9% (<2.0%).

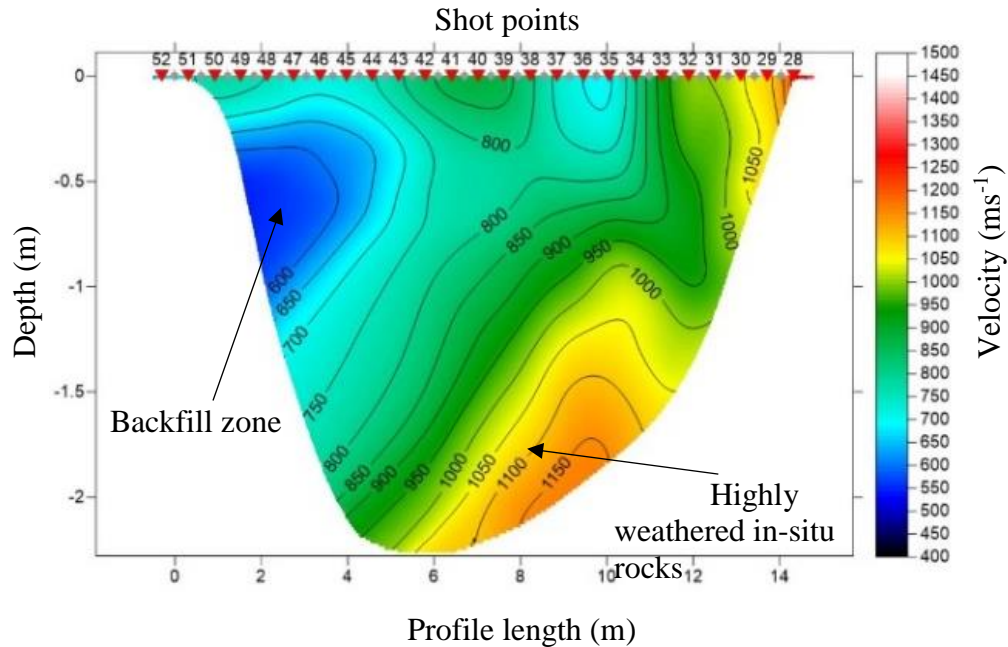


Figure 30: Study area 1 (Road cut site): Line 2 tomogram.

Black and blue zone (up to 600m/s) are representing the velocity through the backfill zone which is very loose medium. Line 2 is showing the highly weathered zone of in-situ rocks as last few geophones are closer to the cut-slope (≥ 1000 m/s).

Velocity tomogram from the second study area

The first line is based on horizontally averaged DeltatV model and within 20 WET iterations, a reliable solution has been obtained. Wavewidth is 1.8% of central frequency 50Hz and RMS error is 1.1% (<2.0%).

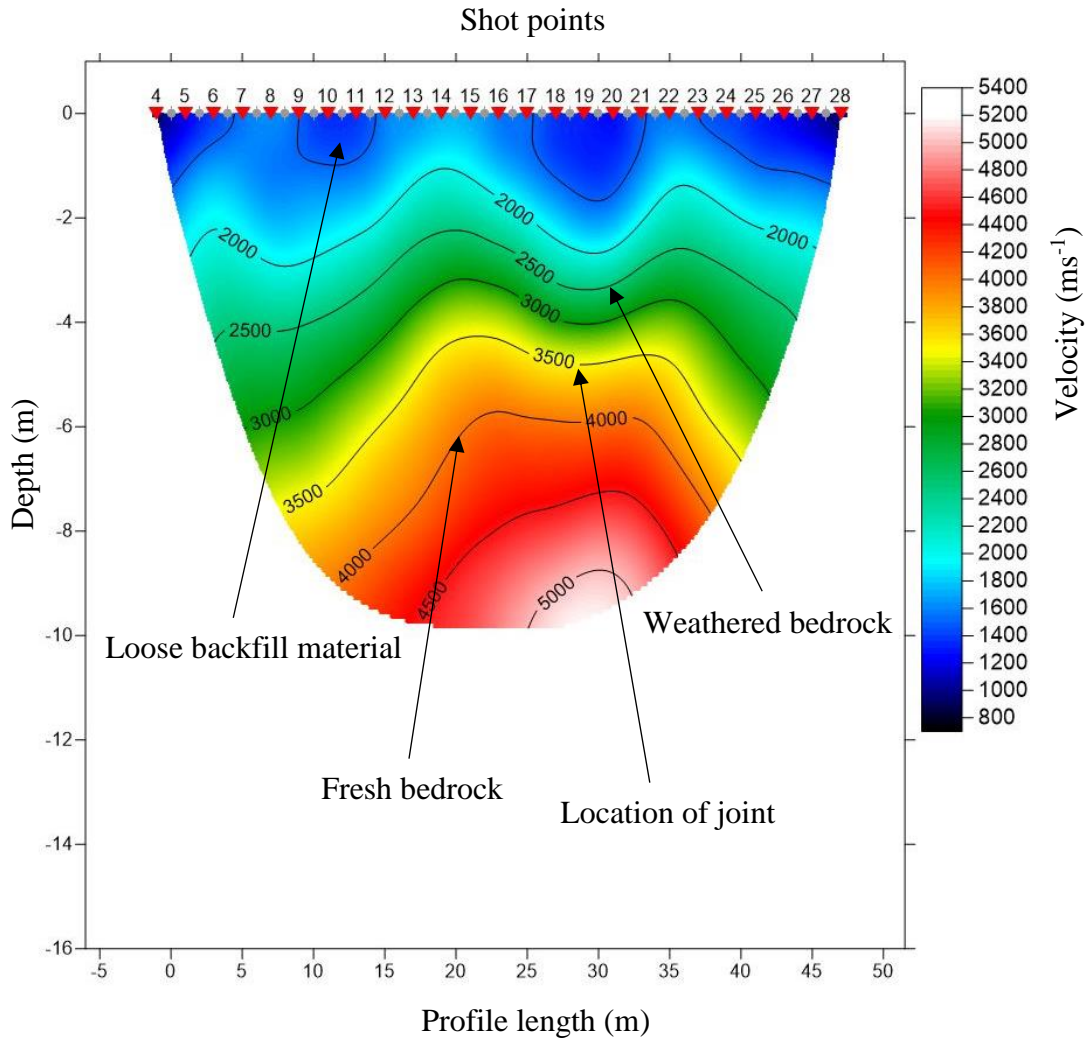


Figure 31: Study area 2 (Dolomite quarry), Intersection 1: Line 1 tomogram.

The second line is also based on horizontally averaged DeltatV model and within 100 WET iterations, a reliable solution has been obtained. Wavewidth is 1.8% of central frequency 50Hz and RMS error is 2.0% (=2.0%).

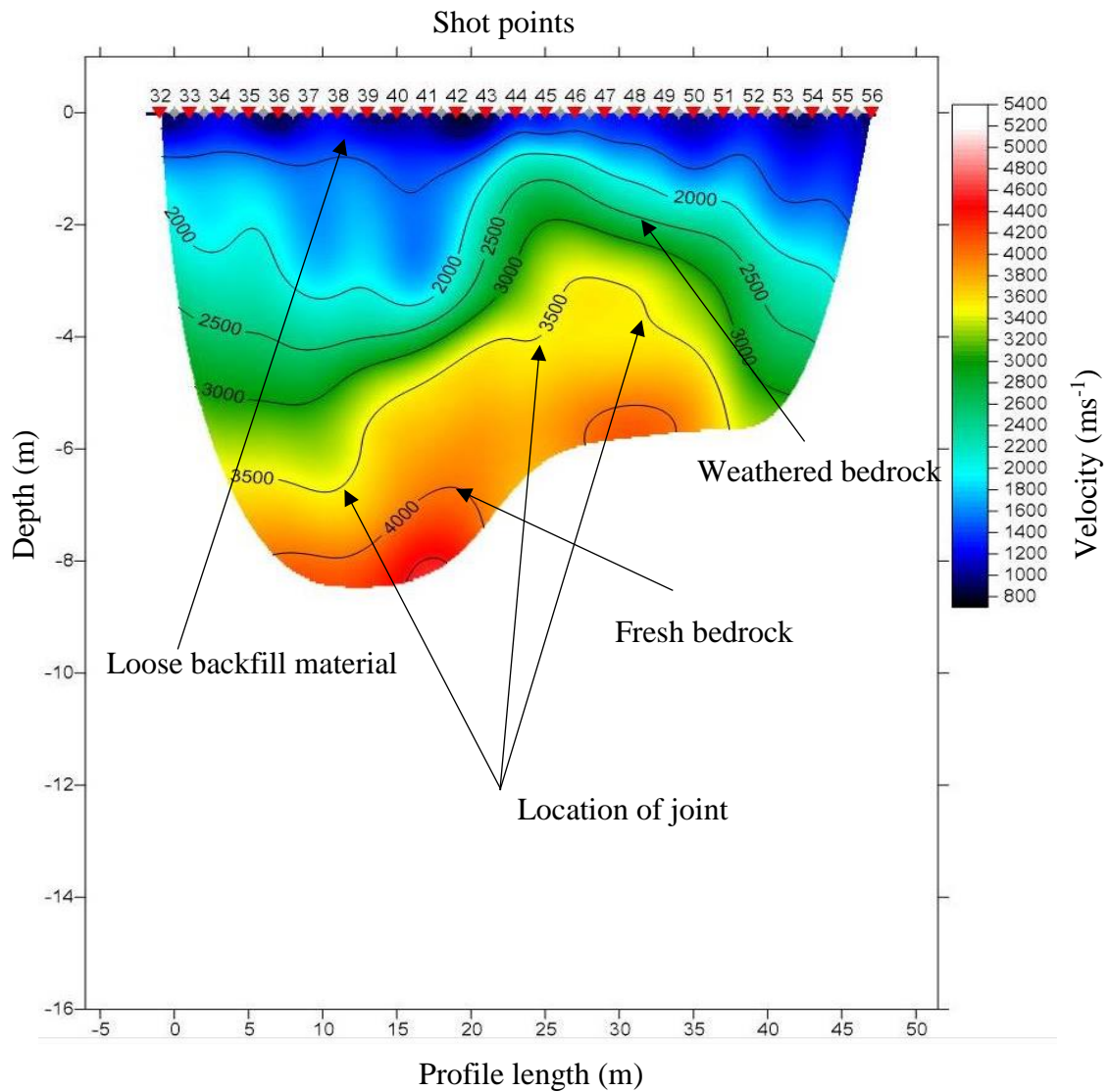


Figure 32: Study area 2 (Dolomite quarry), Intersection 1: Line 2 tomogram.

The third line is based on horizontally averaged DeltatV model and within 20 WET iterations, a reliable solution has been obtained. Wavelength width is 2.2% of central frequency 50Hz and RMS error is 2.2% ($>2.0\%$).

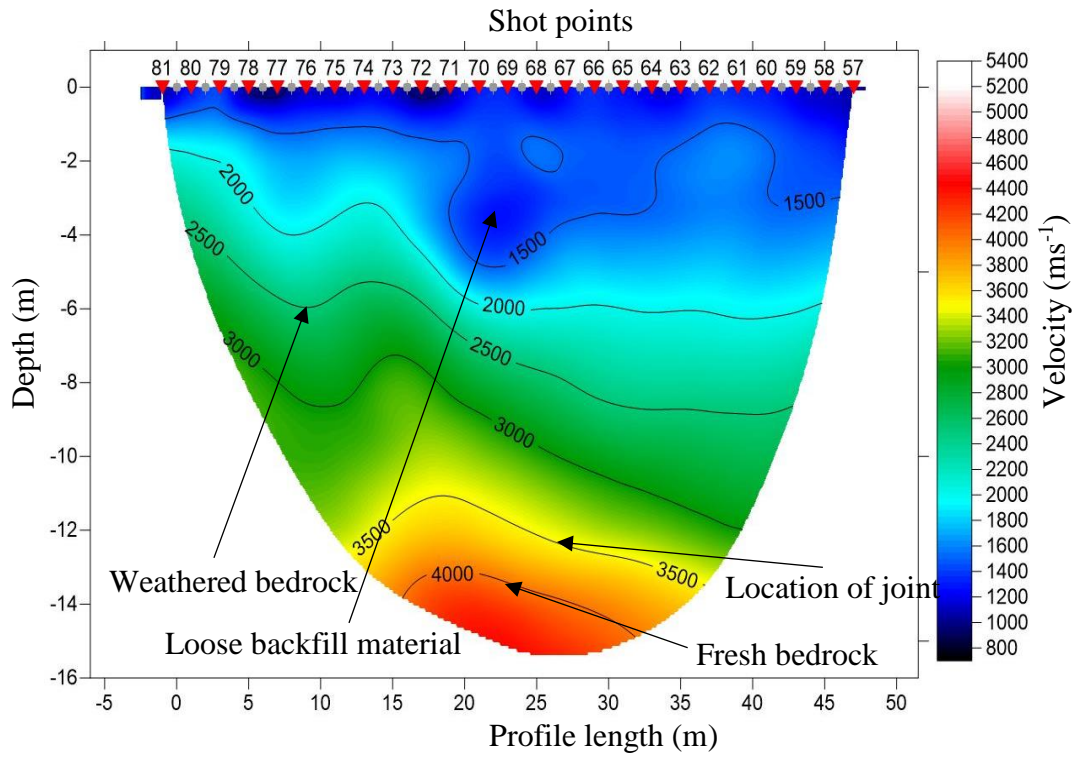


Figure 33: Study area 2 (Dolomite quarry), Intersection 2: Line 3 tomogram.

Finally, the fourth line is based on horizontally averaged DeltatV model and within 20 WET iterations, a reliable solution has been obtained. Wavewidth is 2.3% of central frequency 50Hz and RMS error is 2.2% ($>2.0\%$).

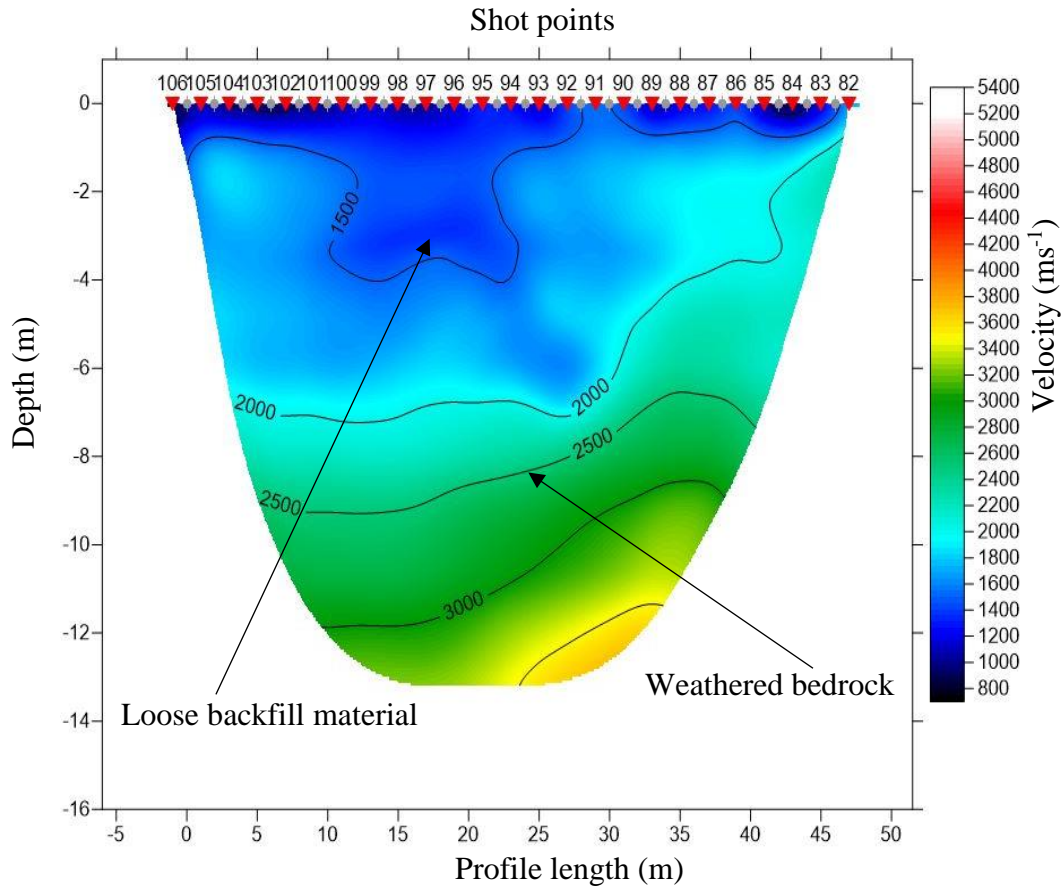


Figure 34: Study area 2 (Dolomite quarry), Intersection 2: Line 4 tomogram.

For all the tomograms from the quarry, the 1500m/s contour line can be interpreted as a boundary between loose backfill material on the top and compact material below. The 4000m/s velocity contour line represents the fresh rock and the degree of weathering is representing by 2000m/s, 2500m/s and 3000m/s velocity contour lines (Mavko, 2005). The 2000m/s contour represents the highly weathered dolomite and 3000m/s represents the very low weathering condition.

3D fence diagram (Velocity)

The acute angle between these lines is 88° . Both of the lines have a length of 14.63m and depth around 2.25m. The lines have intersected at 13th geophones(middle).

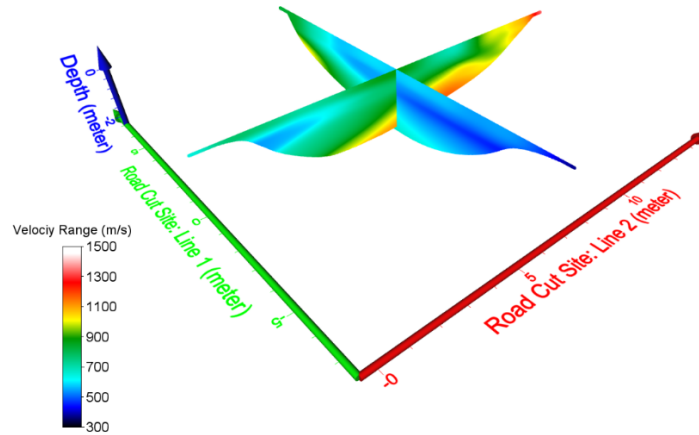


Figure 35: Study area 1 (Road cut site), Velocity fence diagram.

The acute angle between these lines is 85° . Both of the lines have a length of 48m and depth varied from 8-10m. The lines have intersected at 19th geophones.

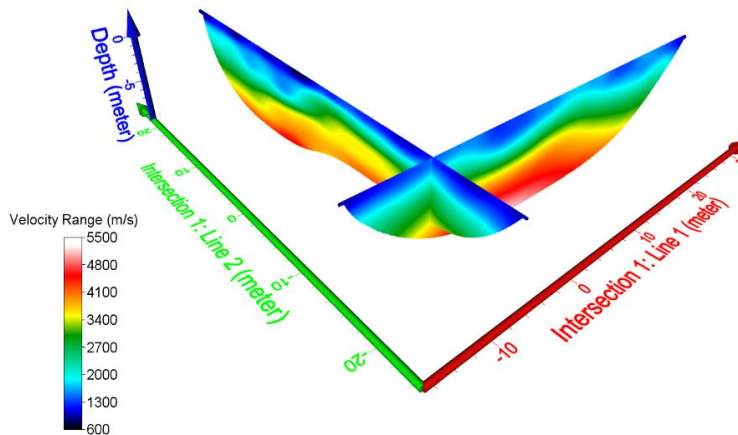


Figure 36: Study area 2 (Dolomite quarry), Intersection 1: Velocity fence diagram.

The acute angle between these lines is 88° . Both of the lines have a length of 48m and depth varied from 13-15m. The lines have intersected at 13th geophones.

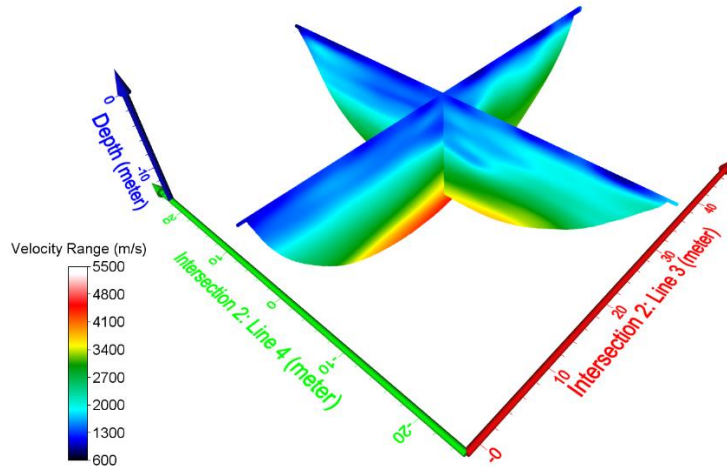


Figure 37: Study area 2 (Dolomite quarry), Intersection 2: Velocity fence diagram.

In the second area at first intersection, bedrock is shallower towards the south. Both lines have backfilled zone on top overlying bedrock.

3D fence diagram (Rock mass quality, Q)

Very low Q value on the top and gradually increase at bottom.

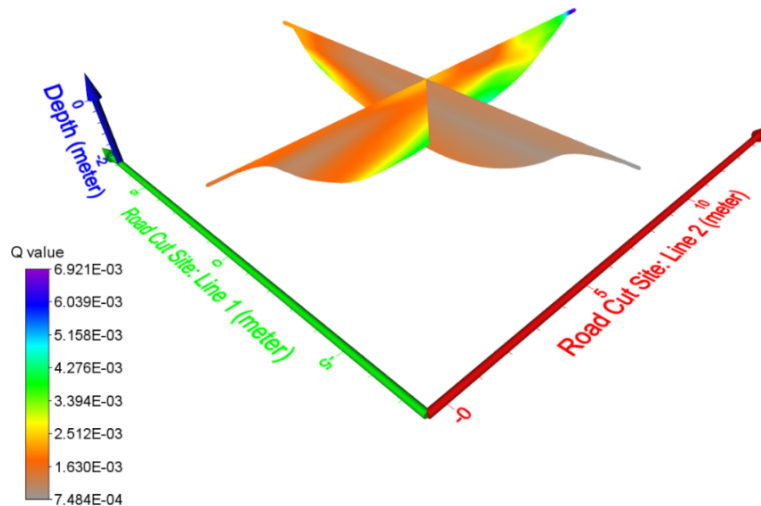


Figure 38: Study area 1 (Road cut site): Fence diagram of Q value (Rock mass quality,

Q).

In the second area, Q value is larger even from the largest value of the first area and it gradually increases in the middle. As soon as, the wave reached the bedrock, it rose up quickly.

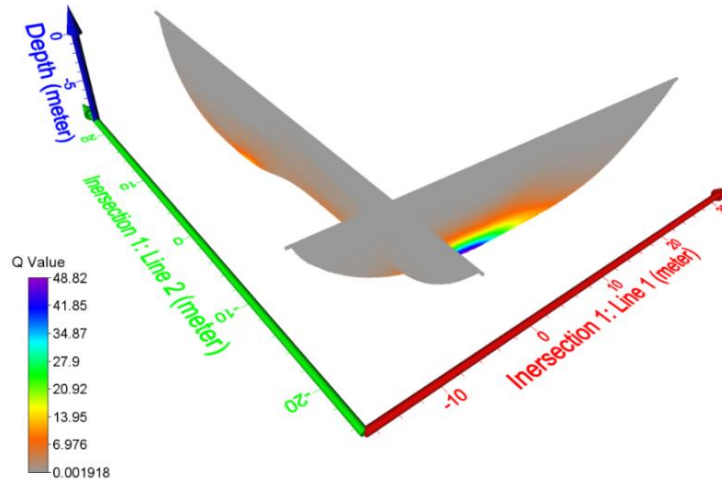


Figure 39: Study area 2 (Dolomite quarry), Intersection 1: Fence diagram of Q value (Rock mass quality, Q).

But in the second intersection, it didn't rise that much as it did in the first one. Largest Q value here was found around 10 at the bottom.

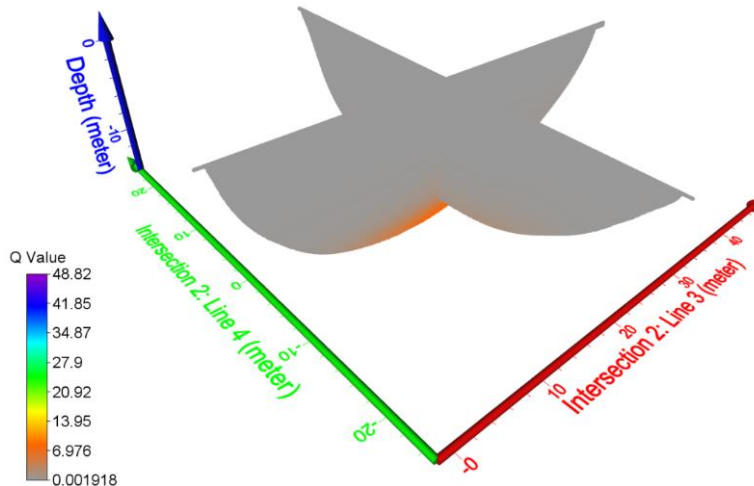


Figure 40: Study area 2 (Dolomite quarry), Intersection 2: Fence diagram of Q value (Rock mass quality, Q).

CHAPTER 7

DISCUSSIONS AND CONCLUSIONS

Discussion

In the first area, none of the profiles reached the bedrock. From the velocity fence diagram of the first area (Figure: 35), area is more compact along line 1 than line 2 and in the line of intersection, the velocity anisotropy is around 300m/s. This much anisotropy is normal for very loose material like soil covering on top. Here, the loose zone is located near the fill slope and towards the north (Figure: 25) the ground is more compact. In-situ rock is shallower near the cut-slope and deeper towards fill slope (Figure: 25). These features of the first area are displaying the velocity anisotropy due to the varying compactness of the fill. This varying compaction is due to the way this area has been filled e.g. dumping materials from north to south and pushing them along the same direction.

In the second area, the depression on the bedrock (4000m/s contour line) is possibly because of the location of profile over joints (Figure: 31, 32 and 33). The joint/fault location is indicated by the depression on the contour lines (Zelt et al. 2013). Line 1 might cross over a joint of the major joint set. The southern part of this area has been used to process the materials, so they have prepared that part for their own convenience. That gave that part a shape like a basin. Over the course of time, the whole area has been filled with rock fill material. On the fence diagram (figure: 36), no visible mismatch in velocity has been identified on the first intersection and thus

no velocity anisotropy exists there. Most probably this intersection ran obliquely over both anisotropy planes or at least major anisotropic plane. The bedrock is deeper below the second intersection. Line 4 barely touched the fresh rock. As the first intersection suggested a dipping direction toward the south and second intersection supported this suggestion. The southern part of the survey area has been used to grind and break the material, so, a basin-shaped topography is observed. A visible mismatch in velocity (around 1000m/s) in the second intersection indicated an existing velocity anisotropy below (figure: 37). The amount of anisotropy, which has been observed in figure: 37 is common at the location of bedrock. Bedrock rose up about 4m in Line 3 relative to the Line 4. This is because Line 3 ran along with the major joint set and Line 4 ran perpendicular to it. Also, Line 3 mostly ran over bedrock and whereas Line 4 barely touched bedrock as it is deeper here.

The following figure: 41 shows the observed distribution of joints in the second area. The major joint sets are drawn based on the observation from face 1 and the inferred joint sets are drawn from face 2 observation. Both figure: 26(3) and figure: 26(4), are representing the face 1 in the following figure which is accessible outcrop here. So, the existence of major joint sets can be supported by figure: 26(3) and figure: 26(4). From the field observation, major joint sets are oriented almost normal to face 1. As face 2 was inaccessible due to terrain condition, it has been inferred that there is another joint set orienting almost normal to the face 2. In a sedimentary sequence, the existence of two orthogonal joint sets is quite normal. Also, this area is a part of Black Warrior foreland basin and two perpendicularly intersected fault systems: Ouachita fold thrust-belt and Appalachian fold-thrust belt, are responsible for the creation of this structure. So, two normal joints sets can be expected in this area and also, in sedimentary strata this kind of joint systems is as usual.

From the analysis of tomograms, two normal joint sets have been inferred to exist. However, the predicted joint sets have been interpreted to be rotated by around 15° anti-clockwise from the pattern observed in the field. The predicted pattern has been shown in figure: 42. The white solid lines are representing the major joint sets and white dashed lines are representing the inferred joint sets. From the structural point of view, this amount of deviation is unusual; however, in a seismic refraction survey, this deviation is quite normal. As from the picking first arrival to the tomogram interpretation, this method does not produce a single unique answer. First picks and adjusting by several iterations depend on experience as well as interpretation. The software used in this study to analyze seismic refraction data is based on some assumptions and sometimes the user has to compromise with these assumptions. The method itself possesses a non-unique nature which may puzzle the user in interpreting the results (Palmer, 2010). All of these uncertainties add up in the final results and may cause the observed deviation.

Rock mass quality Q has been calculated using equation (2) (Barton et al., 1974). For the first study area, the surface quality is below exceptionally poor-quality rocks (0.001) (Appendix) which is indicating the very loose materials. The velocity contour lines representing 1000m/s and above can be attributed to the highly weathered and loose top surface of the in-situ rock near the road cut. Again, exceptionally poor-quality rocks were on the surface in the second study area as both areas have been created in the same way. The quality of soil cover in both areas is similar; very loose materials thus have very low Q value. As soon as the seismic wave reached the bedrock, quality increased quickly (1 and above). A quarry is a more suitable place over road-cut for this type of survey because a quarry allows the survey to be conducted on a larger area, which is one criterion of this study. Preliminary reconnaissance can be done using Google Map. To enter into the quarry; special permission, necessary attire like steel toe boots, helmet, goggles, etc. and a



Figure 41: Observed joint system.

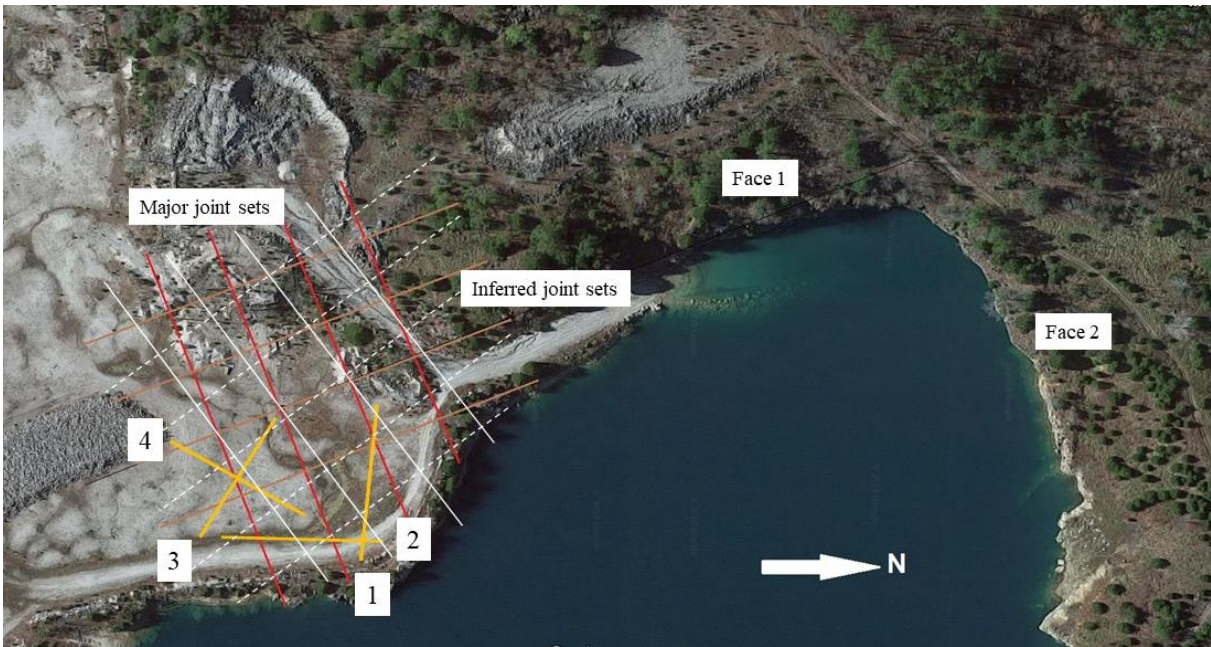


Figure 42: Predicted joint system (Both white solid and dashed lines).

short training are needed. Arrangement of all of these may take some time, so this should be put into consideration. For a better coupling of geophones with the hard ground, the use of clay-mix or plaster is a good choice. Besides velocity measurements, Q value determination is an important aspect of this study.

From the field observation (figure: 26), rock mass quality Q has been calculated and V_P has been derived from these values using equations (1) and (2). Based on field observation, following values for determining the Q have been estimated:

Table 4: Rock mass quality, Q parameters

Parameters	Estimated Value
RQD	90-10
J_n	4
J_r	1.5
J_a	2-4
J_w	1.0
SRF	2.5

Using the above values and equation (1), the range of values of rock mass quality, $Q = 3.375 - 7.5$ has been obtained. Then, using equation (2) the range of values of $V_P = 4.03 - 4.38$ km/s has been calculated. The back-calculation attributes the 4000 m/s contour line as fresh bedrock which is perfectly consistent with our tomograms. As every ten-fold change in Q values changes the V_P by 1 km/s and the estimated Q does not change that much. So, V_P falls within a short-range and similar range has been observed in the tomograms.

Obtaining real data for Q parameters from the field directly is more appropriate than both the estimated one and the one derived from an empirical equation. The equation used here is a trend line from numerous data points but still, it gives Q value on the line rather the exact one. Also, tomograms are subjective and vary with experience of the user. Thus, the derivation of Q from P-wave velocity lacks its significance if it cannot be supported by its field measurement. To solve this, all parameters except RQD can be obtained directly from the field. Samples can be brought to the lab to run core and measure RQD. In case of absence of such facilities, the following relations can be used to estimate RQD (Palmström, 1982).

$$RQD = 115 - 3.3 J_v \quad 16$$

Where, J_v represents the number of joints per cubic meter or the volumetric joint count and $RQD = 100$ for $J_v < 4.5$.

Conclusions

The seismic refraction method has proven to be useful in identifying rock mass anisotropy if two criteria are met: seismic waves must reach bedrock and there must be an outcrop near the survey area to show the joint properties. This method is very effective if the area has a single dominant joint set. The areas having two dominant joint sets require accessible outcrops or cut-faces to obtain necessary rock mass data.

In addition to identifying rock mass anisotropy, this method is also useful to identify the randomness in compaction in the subsurface (first study area).

P-wave velocity has been calculated in two ways: Using the seismic refraction method and from the estimated Q value using equation (1). Also, the Q value has been calculated here in two ways: From the P-wave velocity using equation (1) and from the field observation using equation

(2). The estimation of Q value has produced a range of V_P that is not far off the tomograms. Further improvement of this work can be done by collecting the rock mass data from the outcrop, then calculating the Q value and making a comparison between these two values coming from two different sources.

REFERENCES

- Ackermann, H. D., Pankratz, L. W., & Dansereau, D. (1986). Resolution of ambiguities of seismic refraction traveltimes curves. *Geophysics*, 51(2), 223-235.
- Armstrong, T., McAteer, J., & Connolly, P. (2001). Removal of overburden velocity anomaly effects for depth conversion. *Geophysical Prospecting*, 49(1), 79-99.
- Arsdale, R. V. (2009) *Adventures Through Deep Time: The Central Mississippi River Valley and Its Earthquakes*, Boulder, CO: The Geological Society of America, Inc.
- Barton, Nicholas, Lien, R., & Lunde, J. (1974). Engineering classification of rock masses for the design of tunnel support. *Rock Mechanics*, 6(4), 189-236.
- Barton, Nick. (1991). Geotechnical design. *World Tunneling*, 410-416.
- Barton, Nick. (1995). The influence of joint properties in modelling jointed rock masses. *8th ISRM Congress*. International Society for Rock Mechanics and Rock Engineering.
- Barton, Nick. (2002). Some new Q-value correlations to assist in site characterization and tunnel design. *International Journal of Rock Mechanics and Mining Sciences*, 39(2), 185-216.
- Boggs Jr, S. (2014). *Principles of sedimentology and stratigraphy*, Upper Saddle River, NJ: Pearson Education.
- Bohara, P., Rhodes, R. A. G., Oyan, M. N. S., Moseley, P. & Aydin, A. (2017). Geophysical Characterization of a Confederate Cemetery. *AEG 60th Annual Meeting*.

- Bradley, D. C., & Kidd, W. S. F. (1991). Flexural extension of the upper continental crust in collisional foredeeps. *Geological Society of America Bulletin*, 103(11), 1416-1438.
- Braile, L. (2010). https://web.ics.purdue.edu/~braile/edumod/waves/WaveDemo.htm#Contents_Top.
- Buchanan, R. S., & Johnson, F. K. (1968). *Bonanza gas field: a model for Arkóma basin growth faulting*, Oklahoma City, OK: Oklahoma City Geological Society.
- Burger, H. R., Sheehan, A. F. & Jones, C. H. (2006). Introduction to applied geophysics. New York, NY: W. W. Norton & Company, Inc.
- Cates, L. M., McIntyre, M. R., Hawkins, W. B., & Groshong Jr, R. H. (2004). Structure and oil and gas production in the Black Warrior basin: Tuscaloosa, Alabama, University of Alabama College of Continuing Studies. In *2004 International Coalbed Methane Symposium Proceedings, Paper*, 440, 34.
- Cherry, B. A. (1990). *Internal deformation and fold kinematics of part of the Sequatchie anticline, southern Appalachian fold and thrust belt, Blount County, Alabama* (Doctoral dissertation, University of Alabama).
- Dockery III, D. T., & Thompson, D. E. (2016). The Geology of Mississippi, Jackson, MS: Mississippi Department of Environment Quality.

- Duellmann, H., & Heitfeld, K. H. (1978). Influence of grain fabric anisotropy on the elastic properties of rocks. *Proceedings 3rd IAEG Congress, Madrid, II (1), Imprime ADOSA, Madrid*, 150-162.
- Eitzenberger, A. (2012). Wave Propagation in Rock and the Influence of Discontinuities (Doctoral Thesis, Luleå University of Technology, Sweden).
- Fossen, H. (2016). *Structural geology*, Cambridge, UK: Cambridge University Press.
- Gebrande, H., & Miller, H. (1985). Refraktionsseismik. *Angewandte Geowissenschaften II*, 226-260.
- Groshong Jr, R. H., Pashin, J. C., & McIntyre, M. R. (2009). Structural controls on fractured coal reservoirs in the southern Appalachian Black Warrior foreland basin. *Journal of Structural Geology*, 31(9), 874-886.
- Grujic, N. (1974). Ultrasonic testing of foundation rock. In *Proc. 3rd Congr. Int. Soc. for Rock Mechanics*, 2(1), 404-409.
- Hatcher Jr., R. D., Thomas, W. A., Viele, G. W. (1989). The Appalachian-Ouachita Orogen in the United States, Boulder, CO: The Geological Society of America, Inc.
- Iliev, I. G. (1966). An attempt to estimate the degree of weathering of intrusive rocks from their physico-mechanical properties. In *1st ISRM Congress. International Society for Rock Mechanics and Rock Engineering*, 109-114.

- Lacefield, J. (2000). *Lost World in Alabama Rocks*, Tuscaloosa, AL: The Alabama Museum of Natural History.
- Lashkaripour, G. R., & Passaris, E. K. S. (1995). Correlations between index parameters and mechanical properties of shales. In *8th ISRM Congress. International Society for Rock Mechanics and Rock Engineering*, 257-261.
- Lecomte, I., Gjøystdal, H., Dahle, A. and Pedersen, O.C. (2000). Improving modelling and inversion in refraction seismics with a first-order Eikonal solver. *Geophysical Prospecting*, 48(3), 437-454.
- Leary, P. C., & Henyey, T. L. (1985). Anisotropy and fracture zones about a geothermal well from P-wave velocity profiles. *Geophysics*, 50(1), 25-36.
- Luo, Y. and Schuster, G.T. (1991). Wave-equation travelttime inversion. *Geophysics*, 56(5), 645-653.
- Lutgens, F. K., Tarbuck, E. J. & Tasa, D. (2006). *Essentials of Geology*, Upper Saddle River, NJ: Pearson Education, Inc.
- Lykoshin, A. G., Yaschenko, S. G., Mikhailov, A. D., Savitch, A. I., & Koptev, V. J. (1971). Investigation of rock jointing by seismo-acoustic methods. *Proc. Syrup. Soc. int. Mechanique des Roches, Nancy*, I-19.
- Mavko, G. (2005). <https://pangea.stanford.edu/courses/gp262/Notes/8.SeismicVelocity.pdf>.

- Mellen, F. F. (1947). Black Warrior Basin, Alabama and Mississippi. *Bulletin of The American Association of Petroleum Geologists*, 31(10), 1801-1816.
- Nunn, K. R., Barker, R. D., & Bamford, D. (1983). In situ seismic and electrical measurements of fracture anisotropy in the Lincolnshire Chalk. *Quarterly Journal of Engineering Geology and Hydrogeology*, 16(3) 187-195.
- Nur, A. (1971). Effects of stress on velocity anisotropy in rocks with cracks. *Journal of Geophysical Research*, 76(8), 2022-2034.
- Oda, M., Yamabe, T., & Kamemura, K. (1986). A crack tensor and its relation to wave velocity anisotropy in jointed rock masses. *International Journal of Rock Mechanics and Mining Sciences & Geomechanics Abstracts*, 23(6), 387-397.
- Palmer, D. (2010). Non-uniqueness with refraction inversion—a syncline model study. *Geophysical Prospecting*, 58(2), 203-218.
- Palmström, A. (1982). The volumetric joint count—a useful and simple measure of the degree of rock jointing. *Proc. 4th Int. Cong. Int. Assoc. Eng. Geol*, 5, 221-228.
- Pike, S. J. & Warren, B. B. (1968). Black Warrior Basin, Northeast Mississippi and Northwest Alabama. *Natural Gases of North America*, 9(2), 1693-1701.
- Rheams, L. J. & Kidd, J. T. (1982). Depositional Setting of the Pottsville Formation in the Black Warrior Basin, Tuscaloosa, AL: Alabama Geological Survey.

- Rhodes, R. A. G., Bohara, P., Oyan, M. N. S., Moseley, P. & Aydin, A. (2017). Geophysical Characterization of a Short Segment of a River Levee. *AEG 60th Annual Meeting*.
- Rhodes, R. A. G. (2018). Geophysical Characterization of a Levee Segment Along the Coldwater River Levee (Unfinished Master's thesis, The University of Mississippi).
- Schuster, G.T. and Quintus-Bosz, A. (1993). Wavepath eikonal traveltime inversion: Theory. *Geophysics*, 58(9), 1314-1323.
- Stapor, F. W., & Cleaves, A. W. (1992). Mississippian (Chesterian) sequence stratigraphy in the Black Warrior Basin: Pride Mountain Formation (lowstand wedge) and Hartselle Sandstone (transgressive systems tract). *Gulf Coast Association of Geological Societies*, 42(1992), 683-696.
- Stearns, R. G., & Marcher, M. V. (1962). Late Cretaceous and subsequent structural development of the northern Mississippi embayment area. *Geological Society of America Bulletin*, 73(11), 1387-1394.
- Telford, W. M., Telford, W. M., Geldart, L. P. & Sheriff, R. E. (1990). *Applied geophysics*, New York, NY: Cambridge university press.
- Thomas, W. A. (1972). Regional Paleozoic stratigraphy in Mississippi between Ouachita and Appalachian mountains. *AAPG Bulletin*, 56(1), 81-106.
- Thomas, W. A., & Drahovzal, J. A. (1973). *Regional Paleozoic stratigraphy of Alabama*. Tuscaloosa, AL: Alabama Geological Society.

- Thomas, W. A. (1985a). The Appalachian-Ouachita connection: Paleozoic orogenic belt at the southern margin of North America. *Annual Review of Earth and Planetary Sciences*, 13(1), 175-199.
- Thomas, W. A., & Sloss, L. L. (1988). *Sedimentary Cover-North American Craton: U.S.* Boulder, CO: The Geological Society of America, Inc.
- Tsidzi, K. E. N. (1997). Propagation characteristics of ultrasonic waves in foliated rocks. *Bulletin of the International Association of Engineering Geology*, 56(1997), 103-114.
- USACE. (1965). "Coldwater River Levee Construction". FOIA Request from.
- Winkelmann, R.A. (1996). Entwicklung und Anwendung eines Wellenfeldverfahrens zur Auswertung von CMP-sortierten Refraktionseinsätzen. Akad. Verlag.
- Wu, S., & Groshong Jr, R. H. (1991). Low-temperature deformation of sandstone, southern Appalachian fold-thrust belt. *Geological Society of America Bulletin*, 103(7), 861-875.
- Wyllie, D. C. (2014). *Foundations on rock: engineering practice*. New York, NY: E & FN Spon.
- Zelt, C.A., Haines, S., Powers, M.H., Sheehan, J., Rohdewald, S., Link, C., Hayashi, K., Zhao, D., Zhou, H.W., Burton, B.L. and Petersen, U.K. (2013). Blind test of methods for obtaining 2-D near-surface seismic velocity models from first-arrival traveltimes. *Journal of Environmental and Engineering Geophysics*, 18(3), 183-194.
- Zoeppritz, K. (1919). On the reflection and propagation of seismic waves. *Göttinger Nachrichten*, 1(5), 66-84.

USDA Web Soil Survey. [https://websoilsurvey.sc.egov.usda.gov /app/ WebSoilSurvey.aspx](https://websoilsurvey.sc.egov.usda.gov/app/WebSoilSurvey.aspx)

“What is a seismic survey?” Park Seismic LLC.

LIST OF APPENDICES

APPENDIX A

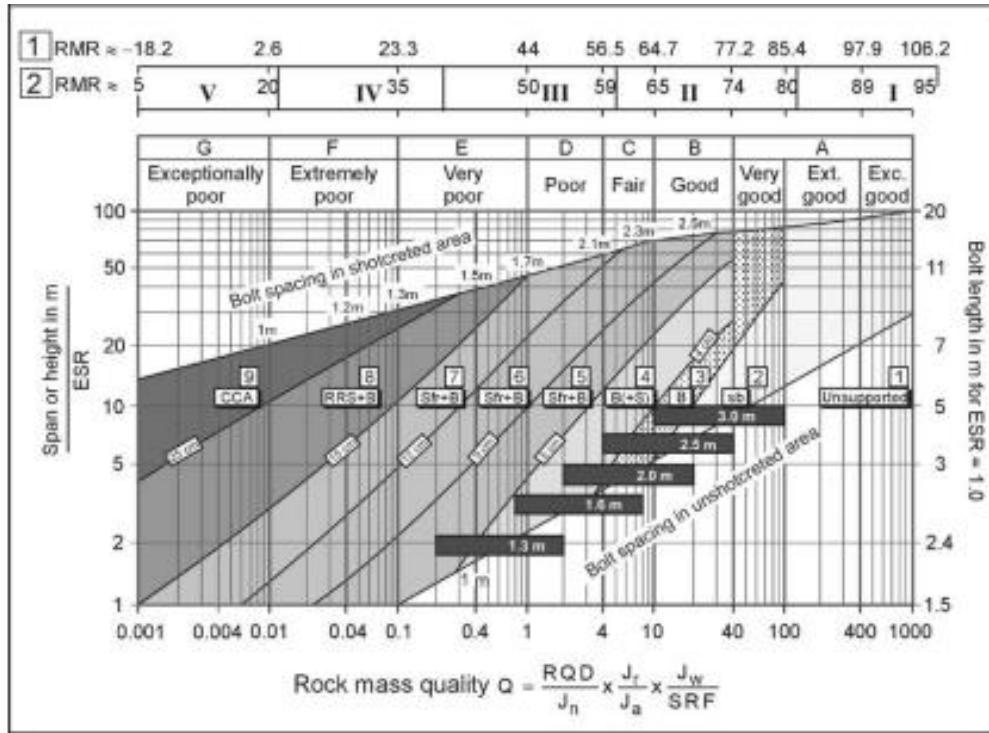


Figure A1: The 1993 updated Q-support chart for selecting permanent B+S(fr) reinforcement and support for tunnels and caverns in rock (Barton, 2002).

APPENDIX B

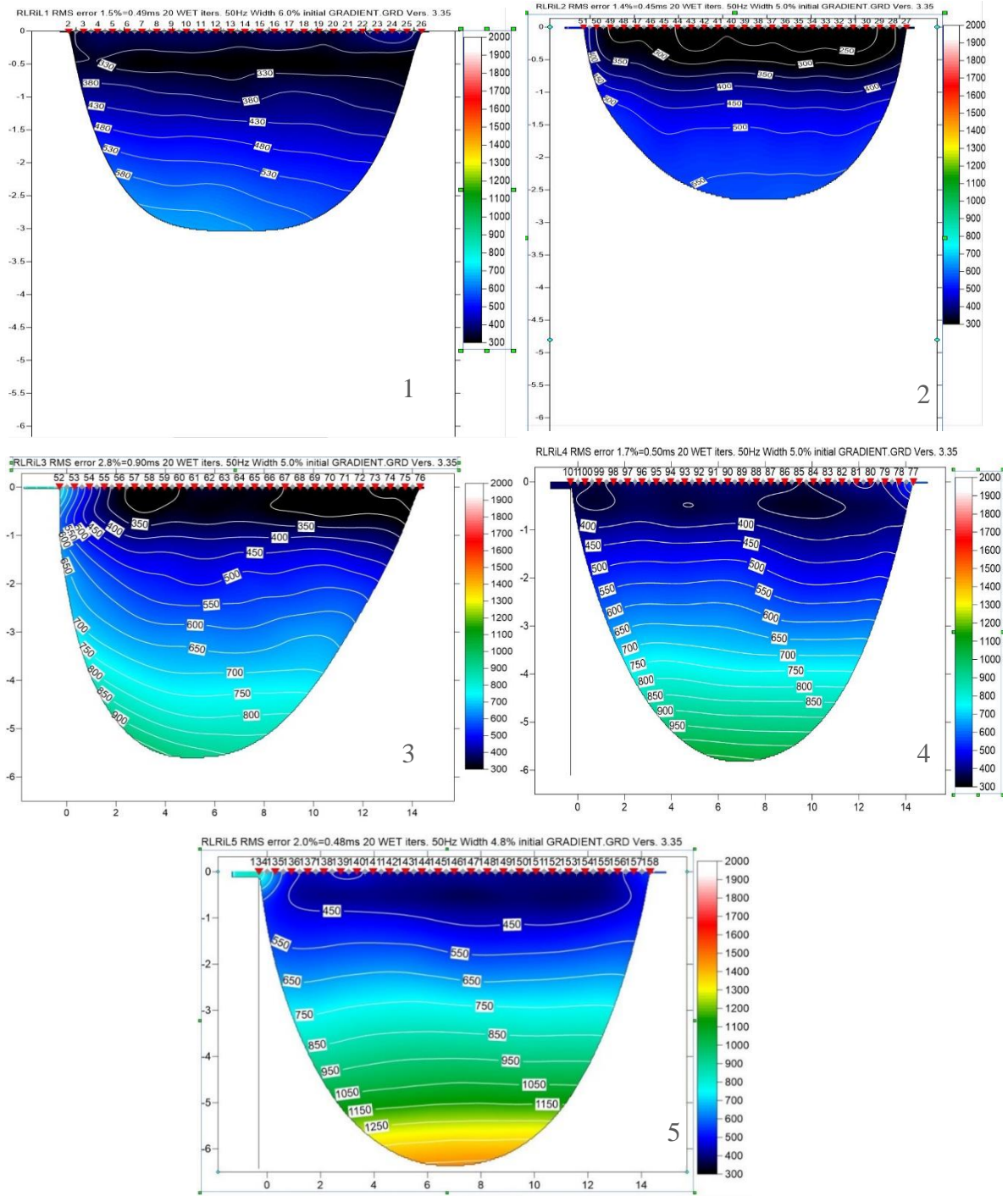


Figure B1: Riverside tomogram

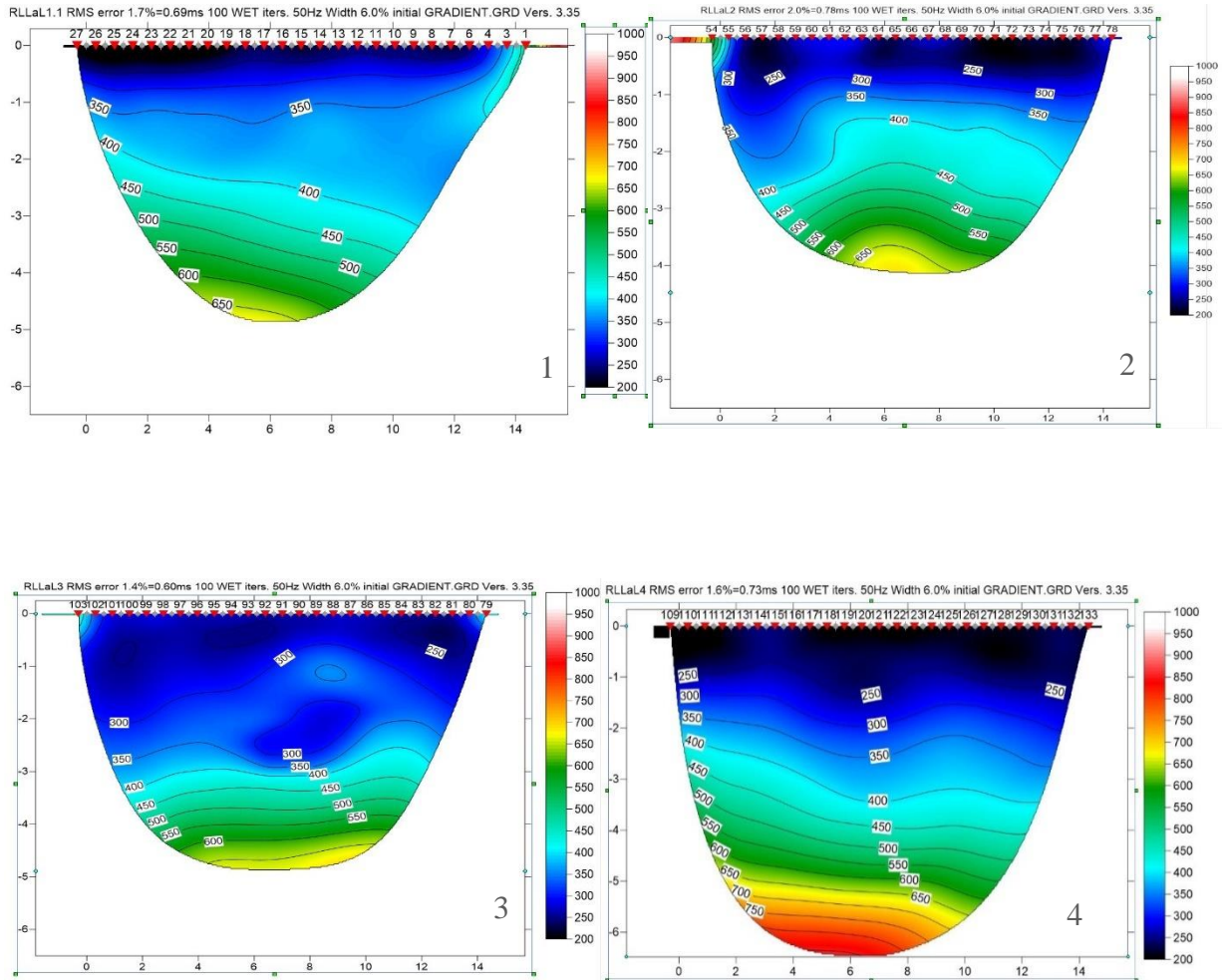


Figure B2: Landside tomogram

APPENDIX C

Creating a new profile

- Select File|New Profile.
- In the File name Section, write QOTL1 and click save.
- Now go to Header|Profile.

Figure C1: Edit profile display

- Set everything as it is on the above image. After setting everything up, click on OK to proceed.

Seismic file import

- After creating a new directory following the above steps, a new directory will be created in C:\RAY32

- After the downloading the data file named under “QOTL1”, copy all the .dat file into C:\RAY32\INPUT.
- In File|Import shots, Select SEG-2 as Import data type, then select select under Input directory like below;
- A new window will pop-up, select the one of the files, preferably the first one then click open.
- Change Default spread type from default 10:360 channels to 1:24 channels.
- Hit Import shots button to import shots, a window may pop-up and click yes and proceed.
- Leave the Layout start [station no.] at 0, only modify the Shot pos. [station no.].

Corresponding shot positions are given at table

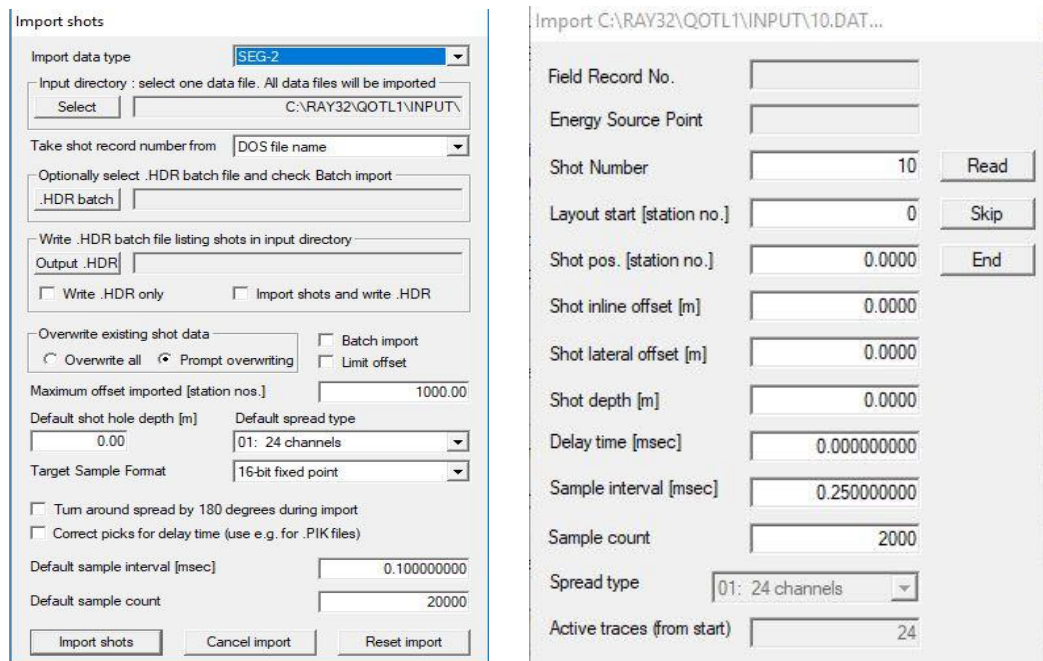


Figure C2: Import shot display (Left) and Shot information display (Right)

- Leave the Import data settings and SEG-2 import settings under File menu as they are.

Pick and review first breaks

- Select Trace|Shot gather, a window will pop-up, click OK. The Shot gather display will appear and first picks can be picked interactively or automatically.

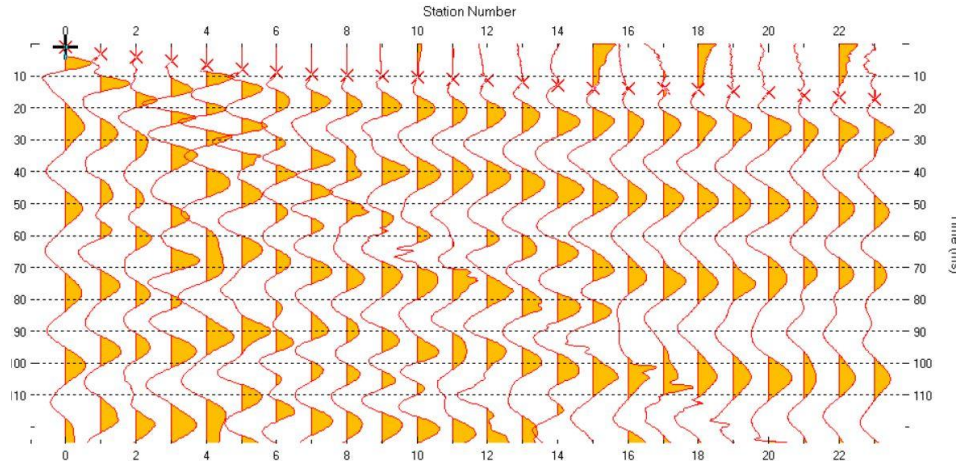


Figure C3: Shot gather display

Table C1: Survey information

OFL1		OFL2		QOT		QOT		QOT		QOT	
_2				L1		L2		L3		L4	
Spacing = 2ft		Spacing = 2ft		Spacing = 2m		Spacing = 2m		Spacing = 2m		Spacing = 2m	
Shot no	Position	Shot no	Position	Shot no	Position	Shot no	Position	Shot no	Position	Shot no	Position
3	23	28	23.5	4	-0.5	32	-0.5	57	23.5	82	23.5
4	22	29	22.5	5	0.5	33	0.5	58	22.5	83	22.5
5	21	30	21.5	6	1.5	34	1.5	59	21.5	84	21.5
6	20	31	20.5	7	2.5	35	2.5	60	20.5	85	20.5

7	19	32	19.5	8	3.5	36	3.5	61	19.5	86	19.5
8	18	33	18.5	9	4.5	37	4.5	62	18.5	87	18.5
9	17	34	17.5	10	5.5	38	5.5	63	17.5	88	17.5
10	16	35	16.5	11	6.5	39	6.5	64	16.5	89	16.5
11	15	36	15.5	12	7.5	40	7.5	65	15.5	90	15.5
12	14	37	14.5	13	8.5	41	8.5	66	14.5	91	14.5
13	13	38	13.5	14	9.5	42	9.5	67	13.5	92	13.5
14	12	39	12.5	15	10.5	43	10.5	68	12.5	93	12.5
15	11	40	11.5	16	11.5	44	11.5	69	11.5	94	11.5
16	10	41	10.5	17	12.5	45	12.5	70	10.5	95	10.5
17	49	42	9.5	18	13.5	46	13.5	71	9.5	96	9.5
19	8	43	8.5	19	14.5	47	14.5	72	8.5	97	8.5
20	7	44	7.5	20	15.5	48	15.5	73	7.5	98	7.5
21	6	45	6.5	21	16.5	49	16.5	74	6.5	99	6.5
22	5	46	5.5	22	17.5	50	17.5	75	5.5	100	5.5
23	4	47	4.5	23	18.5	51	18.5	76	4.5	101	4.5
24	3	48	3.5	24	19.5	52	19.5	77	7.5	102	3.5

25	2	49	2.5	25	20.5	53	20.5	78	2.5	103	2.5
26	1	50	1.5	26	21.5	54	21.5	79	1.5	104	1.5
27	0	51	0.5	27	22.5	55	22.5	80	0.5	105	0.5
		52	-0.5	28	23.5	56	23.5	81	-0.5	106	-0.5
Shot inline offset											
(-1.0 ft)											

- Use F7/F8 to shift among shots, Ctlr+F1/F2 to zoom in/out the traces and Shift+F1/F2 to zoom in/out along the station number, Shift+PgUp/PgDn to move over zoomed section along the station number and F1/F2 to zoom in/out along time axis.
- In Processing| Bandpass filter, select Low corner frequency 8Hz and High corner frequency 20Hz to remove the noises from the noisy traces. Most traces can be picked easily without applying any filter.
- Subsurface does not vary much and picks between adjacent shots should not varies much. Also, picks between adjacent shots should be consistent in nature.
- Trace|Offset gather display does not useful for us to reciprocity principle. As our shot was not on the geophone location, so, this display will not help us to check the consistency among first arrivals.
- Check the consistencies among shots in Refractor|Shot breaks display. This display a kind of time-distance graph. Image below.

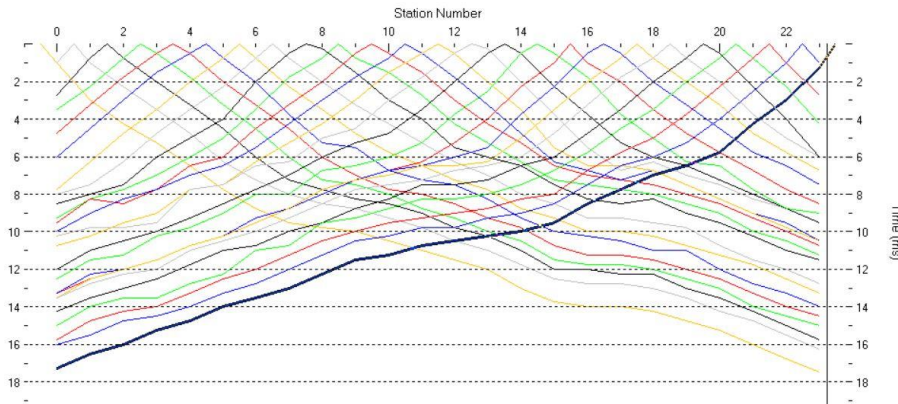


Figure C4: Shot breaks display

WET tomography with Smooth Inversion

- Select Smooth invert|WET with 1D-gradient initial model. This will create a horizontally averaged 1D initial model and call Surfer® to display the initial model. Then a window will appear and ask for permission to run default WET tomography. Allow WET tomography with default option by hitting Enter button. After 20 iterations the process will stop and ray coverage and tomography will be displayed in Surfer®.
- The allowable RMS error is less than 2%. If this goes more than that go to Trace|Shot gather and Refractor|Shot breaks to see the misfit between the forward model and user picks. The red one denotes to user picks and blue one for synthetic model. Try to adjust user picks accordingly. The synthetic model is based on the user picks, so, don't follow them blindly. As long as, the user picks are correct and consistent, the RMS error should be around 2%.
- The process may go through some iterations, picking the first arrivals and producing tomograms, then adjusting the first arrivals again and later produce another tomogram.

- Increasing the number of iterations from 20 to 100 may decrease the error. But in my case it didn't help much. The number of iteration can be increased in the following window which is located WET tomo|Interactive WET tomography. The default model should be GRADIENT.GRD, if not then click the select button and follow this path C:\RAY32\QOTL1\GRADTOMO. But it is a worthy try. Also, increasing the wavepath width increase the robustness by removing the artifacts but offers lo-w resolution in tomogram.

Edit WET Wavepath Eikonal Traveltime Tomography Parameters

Specify initial velocity model
 C:\RAY32\QOTL2\GRADTOMO\GRADIENT.GRD

Stop WET inversion after
 Number of WET tomography iterations : iterations
 or RMS error gets below percent
 or RMS error does not improve for n = iterations
 or WET inversion runs longer than minutes

WET regularization settings
 Wavepath frequency : Hz
 Ricker differentiation [-1:Gaussian,-2:Cosine] times
 Wavepath width [percent of one period] : percent
 Wavepath envelope width [% of period] : percent
 Min. velocity Max. velocity m/sec.
 Width of Gaussian for one period [sigma] : sigma

Gradient search method
 Steepest Descent Conjugate Gradient

Conjugate Gradient Parameters
 CG iterations Line Search iters.
 Tolerance Line Search tol.
 Initial step Steepest Descent step

Figure C5: WET parameter display

DeltatV

- I have used DeltatV only for second line in road cut, Hardy, AR. It is always better to avoid this method because the initial model itself contains artifacts which are carried to the tomogram. This can be found in DeltatV|Automatic DeltatV and WET inversion, after clicking this an DeltatV initial model will be generated and a prompt window will appear to ask permission for WET inversion. After clicking yes, WET inversion run with its default parameters.

Appendix II - Surfer®

- After obtaining the desired tomograms in Surfer®, go to Object manager|Image - [VELOITXX.GRD], here XX is the iteration number. In Property Manager, go to General|Colors, select Rainbow2 and set Minimum=400 and Maximum=1500 for OFL1 and OFL2, set Minimum=800 and Maximum=5400 for QOTL1, QOTL2, QOTL3 and QOTL4 and hit OK.
- Go to Object Manager|Contours-[VELOITXX.GRD], here XX is the iteration number. In Property Manager, go to Levels|General, set Minimum contour= 500, Maximum contour=1500, Contour interval= 50 and Major contour every= 1. for OFL1 and OFL2; set Minimum contour= 500, Maximum contour= 5500, Contour interval= 500 and Major contour every= 1. for QOTL1, QOTL2, QOTL3 and QOTL4.
- Go to Object Manager|Left Axis. In Property Manager, go to Scaling|Scaling, set Axis minimum= -2.4, Axis maximum= 0.113976 and Major interval= 0.5 for OFL1 and OFL2 and set Axis minimum= -16, Axis maximum= 0.773635 and Major interval= 2 for QOTL1, QOTL2, QOTL3 and QOTL4.

- Now take screenshots to save your image. As our surfer is a Demo Inversion, we cannot save our image.

Voxler[®]: Velocity fence diagram:

- Before beginning work in Voxler[®], export the velocity file as ASCII file. Go to Grid|Export grid file to ASCII.TXT. Click Select grid file and a new window will pop-up. Select GRADTOMO or TOMO for smooth invert or DeltatV respectively. Select the VELOITXX.GRD file, here, XX is the iteration number. Choose the file that has been used to produce tomogram. Set Min. velocity and Max. velocity according to the velocity range of the profile set in Surfer[®] in Object manager|Image, and then in Property Manager, under General|Colors tab. Click on the Export to .TXT button to export the velocity grid file as a ASCII file. The file will be saved in either GRADTOMO or TOMO.
- Open the Voxler[®], create a new project first from File|New|Project. On the Viewer window a new project is now open.
- Go to File|Import, select one of the velocity files i.e. QOTL1 velocity file. A new window called Data Import Options will appear. Set Start import at= 2 and click OK. This file is now available in the Network Manager. Similarly, import the velocity file of QOTL2. Select Network Manager|QOTL1, then select Property Manager|Worksheet|Edit Worksheet. Select the column E and delete it and do the same for QOTL2.
- Move the cursor on one of files in Network Manager and click the right button. From there select Computational|Transform. A new path is now created between the file and Transform option. Do this for the other file also.

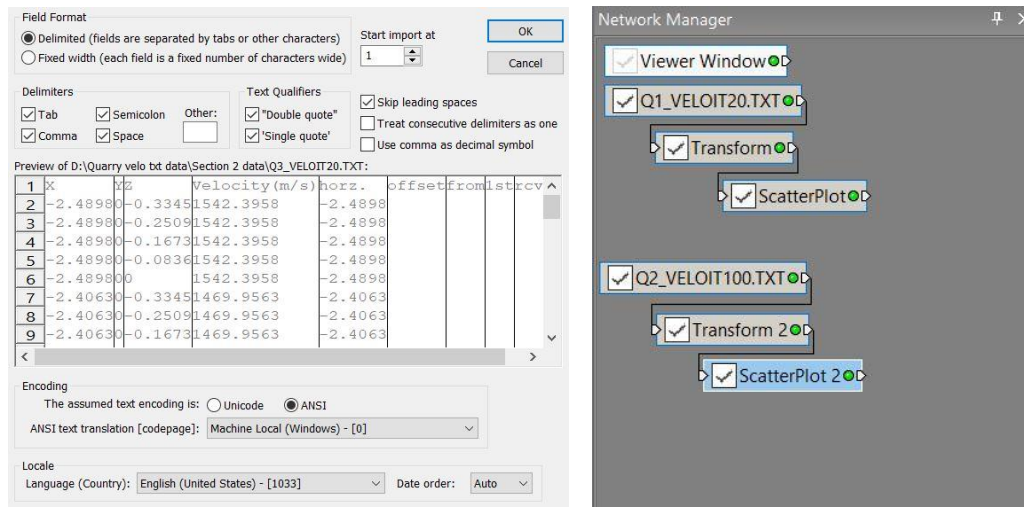


Figure C6: File import display (Left) and Network manager (Right)

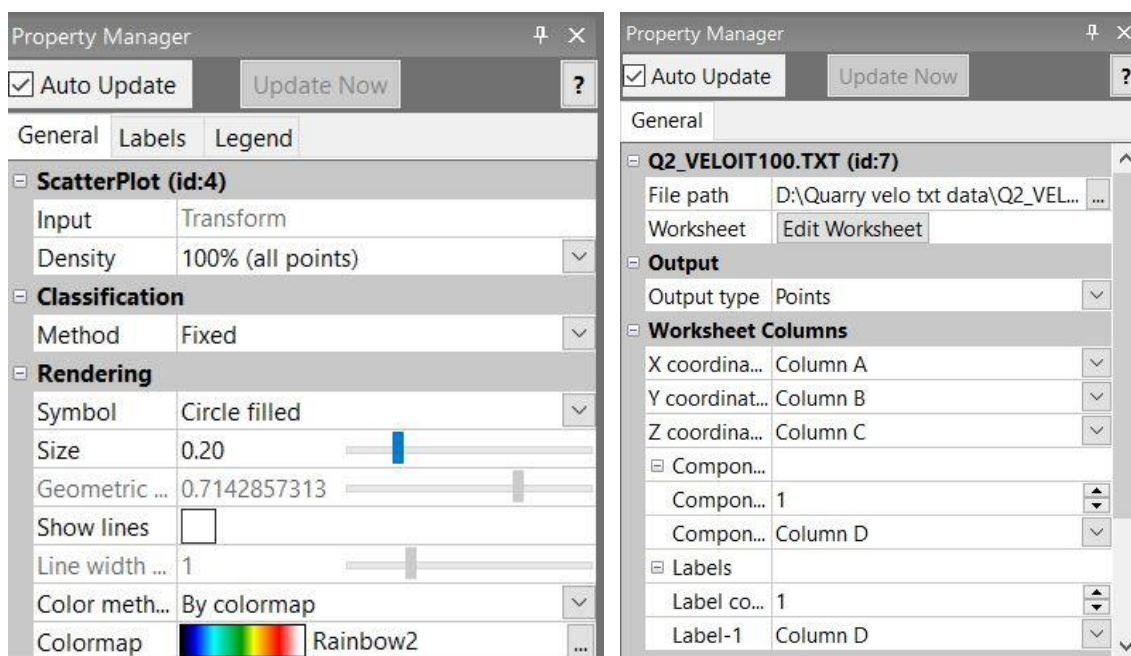


Figure C7: Property manager (for scatter plot: left and for data: right)

- In the Network Manager, select Transform of velocity file for QOTL2. Go to the Property Manager|General. Set the Origin = Custom and set X = 38. Now go to the Property Manager|Transform|Rotation. Set Angel(degree) = 270 and hit Enter.

- Now in the Property Manager, right click on the Transform and select save data. An Export window pop-up, set the File name= QOTL1 and Save as Type= XLSX Excel 2007 spreadsheet (*.xlsx) and hit Save button. Do this for other velocity file under QOTL2 name.
- Open both QOTL1.xlsx and QOTL2.xlsx in excel. Copy all the data from the both file into a new excel sheet and named it Combined intersection 1 velocity and save it as .xlsx format. The column number in the new file will be same as parent files.
- Open a new project and import Combined intersection 1 velocity.xlsx like before. Right click on it on Network Manager and add Transform like before. Right click on Transform and select Graphics Output|ScatterPlot and right click on ScatterPlot in Network Manager, select Graphics Output|Axes.
- In the Viewer window, a fence diagram will appear with XYZ axes.
- Select ScatterPlot in the Network Manager. In Property Manager|General, set Density= 100% (all points). In Property Manager|General|Rendering, set Symbol= Circle filled, then go to the Colormap Editor from Colormap. Select Color Mapping: Rainbow2, set Data Min: 600 and Data Max: 5500 for quarry data and Data Min: 300 and Data Max: 1500 for road cut data.
- In Property Manager|Legend, put ticks by Show legend. Write Velocity chart in the Title under Legend tab. Make Number of labels= 8 in Labels under same tab.
- Right click on the Axes in Network Manager then come to the Property Manager again. Write “Intersection 1: Line 1 (meter)”, “Intersection 1: Line 2 (meter)”, “Depth (m)” in the Title bar of X, Y and Z axis respectively in Property Manager. Put tick by Flip text

horz. for Y-axis and Flip text vert. for Z-axis. Set Cross Y axis at (Y value) = 24.67 and hit Enter.

Q-value fence diagram

- Open Combined intersection 1 velocity.xlsx again. Add a column E for Q value. Use this equation $V_p \approx 3.5(\text{Km/s}) + \log_{10} Q$ to find out Q and put these values in column E. Save the file and exit.
- Now create a new project and import Combined intersection 1 velocity.xlsx file again.
- Select Combined intersection 1 velocity.xlsx in Network Manager. Select Column E in Component-1 in Components and Label-1 in Labels under General tab in Property Manager. Add Transform, ScatterPlot and Axes in Network Manager.
- In Property Manager, set Density: 100% (all points), Symbol: Circle filled and select RainbowReverse in Colormap Editor. Set Data Min: 0.001918, Data Max: 48.82 and select Color: 40% Black corresponding to the Data Min for the quarry data. And, set Data Min: 0.0007484, Data Max: 0.006921 and select Color: 40% Black corresponding to the Data Min for the road cut data.
- Save the images as .bmp file from File|Export, leave the options as they are and click Save.

VITA

Mohammad Najmush Sakib Oyan

Education

B.Sc. in Civil Engineering, (2014)

Bangladesh University of Engineering and Technology (BUET)

Major: Geotechnical Engineering

Professional Experience

Graduate Teaching Assistant, Department of Geology and Geological Engineering,
The University of Mississippi (2017-present)

- Lab Instructor: Rock Mechanics.
- Instructor: Engineering analysis, Engineering Geology, and Sedimentology and Stratigraphy.
Assistant Engineer (Civil), Dhali Enterprise LTD. (2014-2016)
- Cost estimation, Construction management, Structural drawing.